AMERICAN UNIVERSITY OF BEIRUT

MODELLING OF EEG DYNAMICS UNDER ECT USING SQUARE-ROOT CUBATURE KALMAN FILTER

by

KAWTHAR SAEED AL-ALI

A thesis
submitted in partial fulfillment of the requirements
for the degree of Master of Engineering
to the Department of Electrical and Computer
Engineering
of the Faculty of Engineering and Architecture
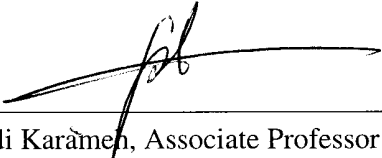at the American University of Beirut

Beirut, Lebanon
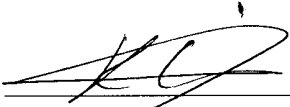May 2014

AMERICAN UNIVERSITY OF BEIRUT

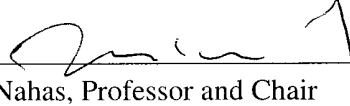# MODELLING OF EEG DYNAMICS UNDER ECT USING SQUARE-ROOT CUBATURE KALMAN FILTER

by

KAWTHAR SAEED AL-ALI

Approved by:

_____ $2\circ - 5 - 2\circ/4$

Fadi Karameh, Associate Professor   Co-Advisor
ECE

_____ $2\circ - 5 - 2\circ(4$

Rouwaida Kanj, Assistant Professor   Co-Advisor
ECE

_____ $2\circ . 5 - /4$

Ziad Nahas, Professor and Chair   Committee Member
Department of Psychiatry

Date of thesis defense: May 12, 2014

AMERICAN UNIVERSITY OF BEIRUT

THESIS, DISSERTATION, PROJECT RELEASE FORM

Student Name: _____
                          Last   First   Middle

◯ Master's Thesis   ◯ Master's Project   ◯ Doctoral Dissertation

☐   I authorize the American University of Beirut to: (a) reproduce hard or electronic copies of my thesis, dissertation, or project; (b) include such copies in the archives and digital repositories of the University; and (c) make freely available such copies to third parties for research or educational purposes.

☐   I authorize the American University of Beirut, **three years after the date of submitting my thesis, dissertation, or project,** to: (a) reproduce hard or electronic copies of it; (b) include such copies in the archives and digital repositories of the University; and (c) make freely available such copies to third parties for research or educational purposes.

_____
Signature   Date

This form is signed when submitting the thesis, dissertation, or project to the University Libraries

ACKNOWLEDGEMENTS

I would like to sincerely thank Professor Fadi Karameh for his support and guidance through my research for the past three years.

I would also like to thank Professor Rouweida Kanj for her valuable advice and encouragement, Professor Ziad Nahas for his insight on the biomedical part and for providing us with the data.

Many thanks to everyone who helped me finish this thesis.

Finally, I wish to show my gratitude to my family and my fiance for their unconditional love and continuous support.

AN ABSTRACT OF THE THESIS OF

Kawthar Saeed Al-Ali   for   Master of Engineering
                               Major: Electrical Engineering

Title: Modelling of EEG dynamics under ECT using Square-Root Cubature Kalman filter

Electroconvulsive therapy (ECT) is a clinical technique used for treating patients with severe drug resistant depression. The therapy consists of administering brief current pulses through two stimulating electrodes placed on the subject scalp thus creating short-lived therapeutic seizure activity in the underlying brain tissue. Despite being a superior treatment method, ECT efficacy and cognitive side effects remain influenced by many parameters including electrode position and configuration as well as the applied current intensity, duration, and polarity. Over the many years, several innovations were introduced in terms of ECT stimulation parameters to reduce side effects while maintaining the antidepressant quality. Importantly, advancement was experimentally driven with limited understanding of the role of different brain areas in initiating, recruiting and maintaining ECT-induced seizures. In this thesis, we propose the use of a nonlinear interaction model to explain multichannel scalp EEG recordings as the outcome for interacting cortical areas, and thus aid in identifying key cortical players in initiating "efficient" seizures. The interaction models are built from modified neuronal population activity models whose dynamics can reproduce basic features of ECT-induced seizures within local areas and across distant cortical areas. The dynamic models are then used to identify the strength and directionality of effective connections between 4 areas of the brain in three various EEG states: normal, ictal and postictal. The Square-Root Cubature Kalman filter, a recently introduced nonlinear estimation technique, is demonstrated to correctly estimate effective inter-areal connection in simulation models. The method is subsequently applied on real EEG recordings obtained in the AUBMC psychiatry department for patients under the FEAST configuration of treatment.

vi

CONTENTS

ILLUSTRATIONS

TABLES

CHAPTER I

INTRODUCTION

Electroconvulsive therapy (ECT) is a method for treating severe, medication-resistant depression where a weak current is passed through two large electrodes resulting in diffused electric fields. The antidepressant efficacy and cognitive side effects of ECT are influenced by many factors including the position of the electrodes on the head, the current intensity, polarity, and electrode configuration. Any variation in these elements affects the threshold for seizure induction and the way the current propagates into the brain. Throughout the history of the ECT, there have been many attempts to reduce its side effects while maintaining its superior antidepressant efficacy. Innovations were made in terms of pulse shape, pulse width, electrode placement and electrical dosage. However, many areas were poorly explored until recently such as the current directionality and the size and shape of the electrodes [1].

ECT side effects are most prominent immediately after a treatment session, when disorientation is noticeable, and learning and memory are compromised. Specifically, ECT weakens retention of newly learned information (anterograde amnesia-AA), and recall of information learned before treatment(retrograde amnesia-RA). The AA produced by ECT usually occurs for short-time however the RA lasts longer and shows temporal gradient, with events occurring closest in time to the treatment both most vulnerable to initial loss and

1

the slowest to return [2].

At the neurophysiological level, the seizures induced by ECT are the result of (a) extensive hyper-activation of underlying cortical neurons and (b) propagation of such activation to distant cortical areas and brain structures. As as stimulus is applied, a substantial electric field is created in the cortical tissue underlying the stimulating electrode which leads to a significant increase in the extracellular current in this tissue. This current, in turn, leads to strong activation of neurons as expressed by vigorous firing of action potentials. The neural firing activity propagates among neurons in the local area as well as to neurons of other distant connected areas (principally by fibers in the white matter). The stimulus-induced increase in firing activity is expressed by increase in synaptic currents in the dendrites of neurons leading to an increase in electric field fluctuations in the tissue and large amplitude deviations in voltage signal recorded at the scalp of the subject, known as the electroencephalogram. Electroencephalographic (EEG) signals are characterized by their amplitude and frequency. The amplitude reflects the peak fluctuations in electrical voltage. At rest, EEG amplitudes range from 10 to 100 μV while during a seizure they can increase to 1000 μV or more. After the seizure, this intense neuronal hyperactivity is followed by a profound inhibitory response, where postictal EEG amplitudes may decrease to $1 - 10 \mu V$. On the other hand, EEG frequency refers to the number of cycles per second and is measured in hertz (Hz). The electroencephalogram is divided mainly into four frequency bands: delta ($0 - 4$Hz), theta ($5 - 7$ Hz), alpha ($8 - 13$ Hz), and beta ($13 - 20$Hz). The commonly recorded EEG signals consist of the summation of multiple

oscillating components at different frequencies. The largest component is referred to as the dominant frequency of the signal [3].

ECT treatment consists of multiple sessions. The first session, called a titration, is aimed at finding the threshold stimulus at which a seizure occurs in patient. An initial stimulus train lasting for one second is first applied and the resultant brain activity (as well as muscle tone) of the subject is monitored. If the seizure doesn't occur then the time duration is multiplied by 2 and so on. When the seizure takes place the amount of charge delivered in *mC* by the train pulse is recorded and is called the seizure threshold. The second session is a treatment session where there is a direct admission of a stimulus that delivers an amount of charge equal to $6\times$ the seizure threshold.

Figure 1 represents the distinctive phases of a seizure [3]. Since treatment sessions are conducted under anesthesia, the first phase to be noted in the EEG signal is a period of slow wave anesthetic-related oscillations which is to be thought of as the baseline activity from which seizures are initiated. As the stimulus is applied, large artifacts are recorded since the magnitude of the applied current (0.5-0.9 A) results in voltages well beyond the physiological range of EEG signals. While this period is rich in dynamics, the artifacts preclude the exact understanding of undergoing activity. After the stimulus, recorded EEG undergoes a period of fast runs and irregular spiking (termed early polyspike in the figure) which subsequently is gives ways to more regular large amplitude lower-frequency spikes with a dominant frequency of (1-5 Hz). At this stage, the seizure is maximally spread over the patient scalp and persists for varying period of time to finally subside (presumably due to autonomous cortical

3
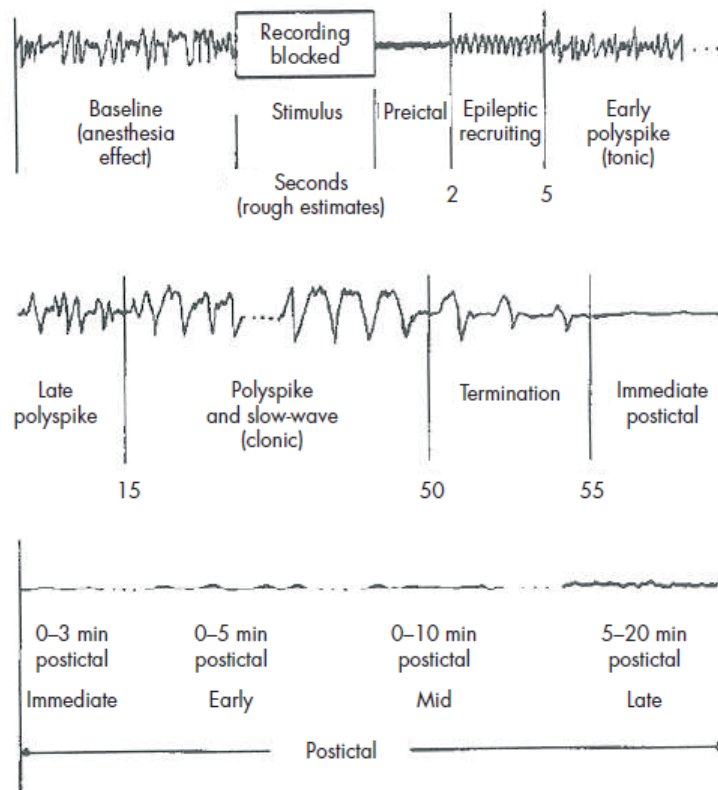
Figure 1: Various phases of a typical ECT induced seizure

inhibition that act to suppress the seizure), thus resulting in the so called post-ictal suppression, a period of significant quenching of activity. The duration of a seizure as well as strength of postictal suppression has been experimentally linked to the effectiveness of an ECT-induced seizures [4]. We are mainly interested in 3 states: baseline (our normal state), polyspike and slow wave (ictal phase of $1 - 4$Hz) and the immediate postictal state.

While many clinical studies have pointed to one or more brain areas a being vigorously activated during an ECT seizure, it remains unclear which cortical structures play the role of drivers and which are actually being recruited

into a seizure. Moreover, and given the increased emphasis placed on post-ictal suppression, it is equally important to isolate the areas that are initially suppressed and the spatial and time progression of this phenomenon.

In this thesis, we propose to utilize biologically inspired models to, first, infer the key areas involved in slow-wave seizure activity and the direction of activity transfer between these areas, and second, to highlight the key areas subjected to post-ictal suppression and the degree of decoupling between such brain areas compared to pre-treatment baseline.

Starting with neuronal population models that were initially proposed by Wendling et al [5] to model spontaneous seizures and later modified by Karameh et al [6] to model externally induced seizures, we will develop a network of models that represent the multi-channel EEG recordings obtained from different brain areas. We will then demonstrate the ability of such models to propagate slow-wave seizures between different brain areas according to a degree of connectivity between these areas. An estimation tool will then be used to fit the obtained models to first simulation data an then to experimentally obtained data for multiple subjects during titration and treatment sessions.

Our model will try to evaluate the parameters representing the connections between these different areas under 3 various EEG states: normal, ictal and postictal. Basically, the Wendling model will be our brain model and will generate the EEG signals. The square-root cubature Kalman filter will be used to tune the connections values of the Wendling model in order to match the generated EEG signals and the real ones from the lab. In summary, The model combines four blocks of the Wendling model interconnected with twelve

5

parameters and tuned by the square-root Kalman filter.

In the next chapter we will give an overview of the neuronal populations models starting with the Jansen model, then the Wendling model for spontaneous seizures followed by the modified Wendling model for induced seizures. Then, we will present the square-root cubature Kalman filter. The fourth chapter will portray development of our multi-area model. Finally, results and discussion of the potential of proposed models will be presented in the fourth chapter.

CHAPTER II

OVERVIEW OF NEURONAL POPULATION MODELS

In order to analyze information processing in the nervous system, a neuronal group study should be conducted. Observation of individual cells activity does not carry enough information for a wide analysis. In addition, a large number of cells is involved in the process creating a precise long-range interactions after inducing some random local activity. Thus, Wilson and Cowan first developed a deterministic model for the dynamics of neuronal populations [7]. Any local population contains excitatory and inhibitory cells and any nervous process is dependent on the interactions between these cells [7]. The electroencephalogram (EEG) is the recording of electrical brain activity recorded by electrodes placed on the scalp. Several mathematical models have been created to simulate this activity [8]. We will present next the Jansen model followed by the Wendling model.

A. The Jansen Model

This section is based on [8] written by Jansen and Rit to describe their mathematical model. Figure 2 shows the nonlinear model of a cortical column. The cortical column is modeled by a population of 'feedforward' pyramidal

7

cells, receiving inhibitory and excitatory feedback from local interneurons and excitatory input from neighboring or more distant columns. The input is represented by a pulse density $p(t)$ which can be any arbitrary function, including white noise.
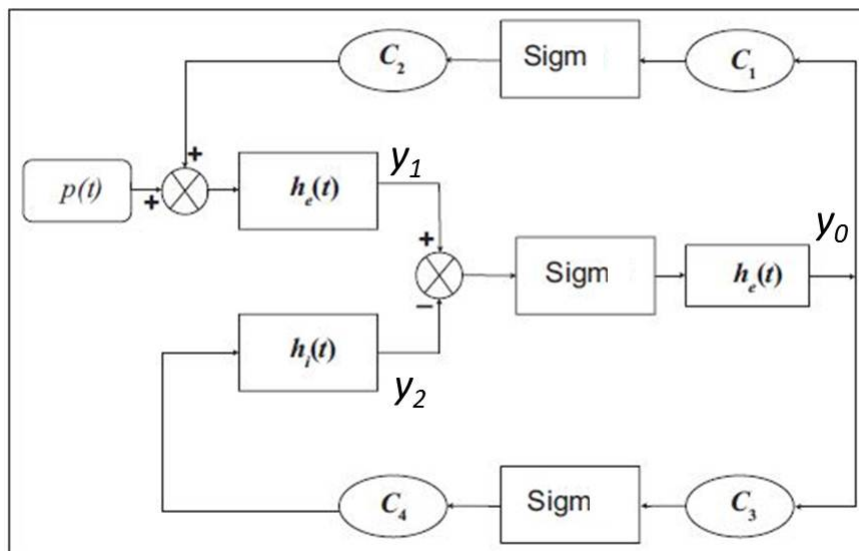
Figure 2: The Jansen Model

Each of the neuron populations is modeled by two blocks: the postsynaptic potential (PSP) and the sigmoid. The PSP block transforms the average pulse density of action potentials coming to the population of neurons into an average postsynaptic membrane potential which can either be excitatory

or inhibitory. The impulse response of this block is given by

$$h_e(t) = \begin{cases} Aate^{-at} & t \geq 0 \\ 0 & t < 0 \end{cases} \tag{1}$$

$$h_i(t) = \begin{cases} Bbte^{-bt} & t \geq 0 \\ 0 & t < 0 \end{cases} \tag{2}$$

for excitatory and inhibitory cases, where A and B are the maximum amplitude of the EPSP and IPSP, and a and b are the lumped representation of the sum of the reciprocal of the time constant of passive membrane and all other spatially distributed delays in the dendritic network. The sigmoid block transforms the average membrane potential of a population of neurons into an average pulse density of action potentials fired by the neurons. The block is represented by the following function

$$\text{Sigm}(v) = \frac{2e_0}{1 + e^{r(v_0 - v)}} \tag{3}$$

with e_0 maximum firing rate of the neural population, V_0 the PSP for which a 50% firing rate is achieved, and r the steepness of the sigmoidal transformation. The last four blocks C_1, C_2, C_3 and C_4 represent the connectivity constants that determines the interaction between the pyramidal cells and the excitatory and inhibitory interneurons.

Each PSP block can be modeled using two differential equations:

$$\ddot{y}(t) = Aax(t) - 2a\dot{y}(t) - a^2 y(t) \tag{4}$$

9

rewritten as

$$
\begin{cases}
\dot{y} = z(t) \\
\dot{z}(t) = Aax(t) - 2az(t) - a^2 y(t)
\end{cases}
\tag{5}
$$

with $x(t)$ and $y(t)$ are the input and the output signals respectively. The following set of six differential equations describe the entire model:

$$
\dot{y_0}(t) = y_3(t)
$$

$$
\dot{y_3}(t) = Aa\, Sigm[y_1(t) - y_2(t)] - 2a y_3(t) - a^2 y_0(t)
$$

$$
\dot{y_1}(t) = y_4(t)
$$

$$
\dot{y_4}(t) = Aa\,\{p(t) + C_2\, Sigm[C1\, y_0(t)]\} - 2a y_4(t) - a^2 y_1(t)
\tag{6}
$$

$$
\dot{y_2}(t) = y_5(t)
$$

$$
\dot{y_5}(t) = Bb\,\{C_4\, Sigm[C_3\, y_0(t)]\} - 2b y_5(t) - b^2 y_2(t)
$$

The model parameters can be set to some specific values found in the literature. The four connectivity constants C_1, C_2, C_3 and C_4 are proportional to the average number of synapses between the pyramidal cells and the excitatory and inhibitory feedback elements. They can be represented as a fraction of one constant:

$$
C = C_1; C_2 = 0.8C; C_3 = 0.25C; C_4 = 0.25C
\tag{7}
$$

The A and B parameters are proportional to the amplitude of the PSP while a and b are inversely proportional to the duration of the PSP. Varying the model parameters results in different outputs like noise, slow periodic activity, and low-amplitude high frequency activity. The following parameters will be fixed

throughout our work:

$$a = 100s^{-1}, b = 50s^{-1}, e_0 = 2.5s^{-1}, v_0 = 6mV \text{ and } r = 0.56mV$$

B. Wendling Model for Spontaneous Seizures

As mentioned in the last section, the Jansen model can generate EEG-like signals. Wendling took this model one step further to simulate seizure-like signals. He tried to model the production of realistic epileptic form activity as a result of imbalance between excitatory and inhibitory synaptic gains [9]. Thus at specific values, the parameters can drive the model into epileptic state. In this case, the epileptic signals (spikes or rhythmic signals) replace the normal EEG signals of the Jansen model. Wendling modified the Jansen model by adding some blocks in order to represent fast EEG activity observed in seizure. A second class of inhibitory interneurons was added to the model in order to raise the kinetics of the system [9]. The impulse responses of the excitatory, slow inhibitory, and fast inhibitory activities are given by the following equations:

$$h_e(t) = Aat\, e^{-at} \tag{8a}$$

$$h_i(t) = Bbt\, e^{-bt} \tag{8b}$$

$$h_g(t) = Ggt\, e^{-gt} \tag{8c}$$
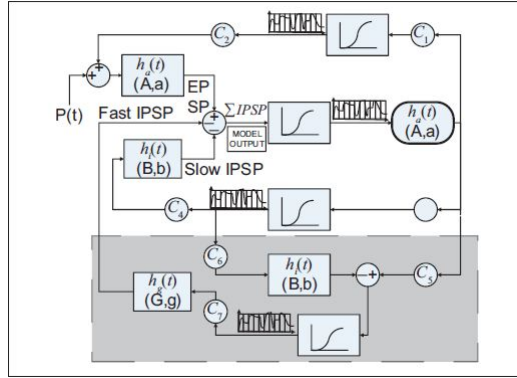
Figure 3: Wendling Model

Figure 3 shows the block diagram representation of the model. The excitatory input $p(t)$ represents the influence from other areas, the output of the model is the postsynaptic activity (EEG signal). Wendling derived a new set of differential equations to model the new system[5].

$$\dot{y_0}(t) = y_5(t)$$

$$\dot{y_5}(t) = Aa\,Sigm[y_1(t) - y_2(t) - y_3(t)] - 2a\,y_5(t) - a^2\,y_0(t)$$

$$\dot{y_1}(t) = y_6(t)$$

$$\dot{y_6}(t) = Aa\,\{p(t) + C_2\,Sigm[C1\,y_0(t)]\} - 2a\,y_6(t) - a^2\,y_1(t)$$

$$\dot{y_2}(t) = y_7(t)$$

$$\dot{y_7}(t) = Bb\,\{C_4\,Sigm[C_3\,y_0(t)]\} - 2b\,y_7(t) - b^2\,y_2(t) \qquad (9)$$

$$\dot{y_3}(t) = y_8(t)$$

$$\dot{y_8}(t) = Gg\,\{C_7\,Sigm[C_5\,y_0(t) - C_6\,y_4(t)]\} - 2g\,y_8(t) - g^2\,y_3(t)$$

$$\dot{y_4}(t) = y_9(t)$$

$$\dot{y_9}(t) = Bb\,Sigm[C_3\,y_0(t)] - 2b\,y_9(t) - b^2\,y_4(t)$$

$$y_{out}(t) = y_1(t) - y_2(t) - y_3(t)$$

12

Where $y_{out}(t)$ is the output EEG signal.

Wendling model can produce six types of EEG signals that represent different activities in the brain by changing the excitation and inhibition synaptic gain parameters (A, B, and G) of the depth-EEG model. These types are: Normal background, sustained discharge of spikes, low voltage rapid activity, slow quasi-sinusoidal activity, sporadic spikes, and slow rhythmic activity[9].

Jansen model can simulate sustained discharge of spikes which is a typical ictal activity. However, it cannot simulate fast EEG activity such as low-voltage rapid discharges observed during seizure. The new model includes a new subset that represents a second class of inhibitory neurons with faster kinetics than the present inhibitory neurons [5]. This addition was made based on the fact that there are two types of gamma-aminobutyric acid $GABA_A$ synaptic responses in pyramidal neurons. $GABA_{A,fast}$ response is near the soma while $GABA_{A,slow}$ is in the dendrites. $GABA_{A,slow}$ cells inhibit both pyramidal cells and $GABA_{A,fast}$ interneurons.

As shown in Figure 3 the new added subset provides somatic inhibition to pyramidal cells. $GABA_{A,fast}$ interneurons receive excitatory input from pyramidal cells and inhibitory input from $GABA_{A,slow}$ interneurons. Thus the model consists of four subsets of neurons, the pyramidal cells,the excitatory interneurons,the slow dendritic-projecting inhibitory interneurons and the fast somatic-projecting inhibitory interneurons. The excitatory input $p(t)$ modelled by Gaussian white noise describes the average density of action potentials from neighboring areas. The EEG output is the summated postsynaptic potentials in activated pyramidal cells.

13
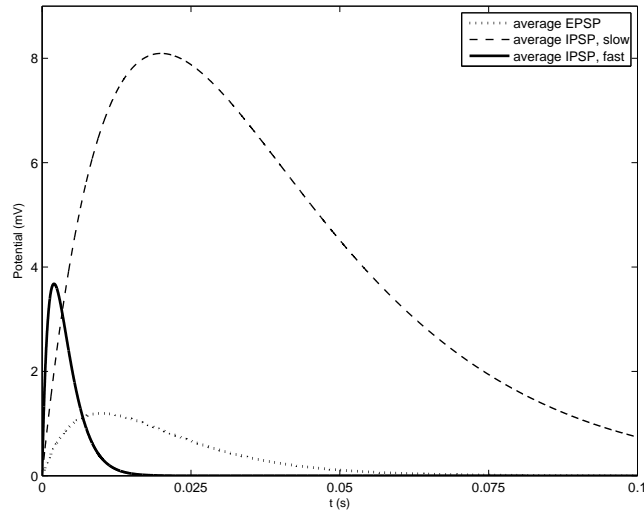
Figure 4: Average postsynaptic membrane potentials: excitatory, slow inhibitory and fast inhibitory obtained from impulse response given by (8)

C. Modified Wendling Model for Induced Seizures

As mentioned in the previous section, the Wendling model represents the connectivity between pyramidal cells, excitatory and inhibitory interneurons. Figure 5 shows the Wendling model of one local area where the basic neural firing element represents the main pyramidal cells. Filled arrows represent fast excitatory connections, filled circles represent fast inhibitory connections and hollow circles represent slow inhibitory connections. The pyramidal cell population are reciprocally connected to (*i*) a population of local excitatory interneurons that provide excitatory feedback to the pyramidal cells (*ii*) a population of fast inhibitory interneurons that provide $GABA_{A,fast}$ somatic inhibition, and (*iii*) a population of slow inhibitory interneurons that provide $GABA_{A,slow}$ dentric inhibition. Thus, rewriting the set of non-linear state-space

14
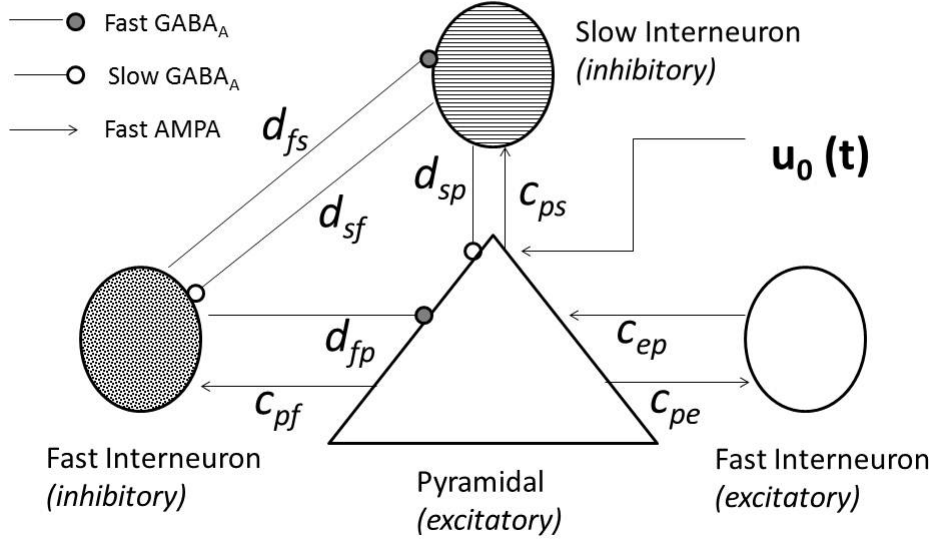
Figure 5: Local Area model

equations in (9) we get:

$$\dot{x}_p(t) = z_1(t) \tag{10}$$

$$\dot{z}_1(t) = AaS\{x_e(t) - x_{is} - x_{if}(t)\} - 2az_p(t) - a^2 x_p(t)$$

$$\dot{x}_e(t) = z_2(t) \tag{11}$$

$$\dot{z}_2(t) = Aa\left[u_0(t) + c_{ep}S\{c_{pe}x_p(t)\}\right] - 2az_2(t) - a^2 x_e(t)$$

$$\dot{x}_{is}(t) = z_3(t) \tag{12}$$

$$\dot{z}_3(t) = Bbd_{sp}S\{c_{ps}x_p(t)\} - 2bz_3(t) - b^2 x_{is}(t)$$

$$\dot{x}_{if}(t) = z_4(t) \tag{13}$$

$$\dot{z}_4(t) = Ggd_{fp}S\{c_{pf}x_p(t) - d_{sf}x_{ii}(t)\}) - 2gz_4(t) - g^2 x_{if}$$

$$\dot{x}_{ii}(t) = z_5(t) \tag{14}$$

$$\dot{z}_5(t) = BbS\{c_{ps}x_p(t)\} - 2bz_5(t) - b^2 x_{ii}(t)$$

$$e(t) = K_{iv}\left(x_e(t) - x_{is} - x_{if}(t)\right) \tag{15}$$

where we have:

$\mathbf{x_p(t)}$: the synaptic current output from pyramidal cell population to all local cells

$\mathbf{x_e}$, $\mathbf{x_{is}}$, and $\mathbf{x_{if}}$: the excitatory input, $GABA_{A,slow}$ inhibitory input and $GABA_{A,fast}$ inhibitory input, respectively, to the pyramidal cells

$\mathbf{x_{ii}}$: the slow inhibitory input onto fast inhibitory cell

$(\mathbf{A}, \mathbf{a})$, $(\mathbf{B}, \mathbf{b})$ and $(\mathbf{G}, \mathbf{g})$: the time profiles of fast excitatory, slow inhibitory and fast inhibitory cells respectively

$\mathbf{u_0(t)}$: the external input assumed to arrive as a firing rate to the local pyramidal population

$\mathbf{d_{m,n}}$ and $\mathbf{c_{m,n}}$: the constants that denote the inhibitory and excitatory connection strengths, respectively, originating from population m to population n and $(m,n) \in \{$p:pyramidal, e:excitatory interneuron, f: fast interneuron, s: slow interneuron$\}$

Finally the voltage trace $e(t)$ is proportional to the over all postsynaptic activity in the pyramidal cell population and is assumed to be representative of the EEG traces of the overall local area.

Based on [6], the model introduced needs more modifications to truly represent seizures induced by overwhelming excitatory drive as is the case in ECT. The Wendling model depends only on the connection parameters. Thus, to make it depend more on the excitatory drive, the local area model is modified by adding a fast inhibitory to slow inhibitory neuron connection with the

16

corresponding change in the dynamics of slow interneurons (((12)))

$$\dot{x}_{is}(t) = z_3(t)$$

$$\dot{z}_3(t) = Bbd_{sp}S\{c_{ps}x_p(t) - d_{fs}x_{if}(t)\} - 2bz_3(t) - b^2x_{is}(t)$$

(16)

CHAPTER III

OVERVIEW OF KALMAN-BASED ESTIMATION

In this chapter, we will give a brief introduction to the basic Kalman filter before presenting the square-root cubature Kalman filter that we will be using throughout our work.

A. Basic Filters

The Kalman filter is a set of mathematical equations that provides a recursive solution to the linear optimal filtering problem. Each updated estimate of the state is computed from the previous estimate and the new input data. Thus, the solution is recursive and there is no need to store the entire past observed data [10]. The aim of the Kalman filter is to estimate the state $x \in \mathbb{R}^n$ of a discrete-time controlled process modeled by the linear stochastic difference equation [11]

$$x_{k+1} = A_k x_k + B u_k + w_k \tag{17}$$

with a measurement $z \in \mathbb{R}^m$

$$z_k = H_k x_k + v_k \tag{18}$$

The control input is $u \in \mathbb{R}^l$. w_k and v_k are independent process and measurement Gaussian noise with zero-mean and covariances Q and R respectively.

$$p(w) \sim N(0, Q) \tag{19}$$

$$p(v) \sim N(0, R) \tag{20}$$

The Kalman filter computes an *a posteriori* state estimation $\hat{\mathbf{x}}_k$ as a linear combination of an *a priori* estimate $\hat{\mathbf{x}}_k^-$ and a weighted difference between an actual measurement z_k and an estimated measurement $H_k \hat{\mathbf{x}}_k^-$ as shown in the following equation:

$$\hat{\mathbf{x}}_k = \hat{\mathbf{x}}_k^- + K(z_k - H_k \hat{\mathbf{x}}_k^-) \tag{21}$$

$(z_k - H_k \hat{\mathbf{x}}_k^-)$ is the residual which we want to make as small as possible in order for the real and predicted measurements to match. K is the gain that minimizes the *a posteriori* error covariance P_k where

$$P_k = E[(x_k - \hat{\mathbf{x}}_k)(x_k - \hat{\mathbf{x}}_k)^T] = E[e_k e_k^T] \tag{22}$$

The Kalman filter maintains the first two moments of the state distribution

$$E[x_k] = \hat{\mathbf{x}}_k$$
$$E[(x_k - \hat{\mathbf{x}}_k)(x_k - \hat{\mathbf{x}}_k)^T] = P_k \tag{23}$$

The state distribution is normally distributed if (19) and (20) are met. The *a posteriori* states estimation reflects the mean of the state distribution and the *a*

posteriori estimate error covariance reflects the variance of the state distribution :

$$p(x_k \mid z_k) \sim N(E[x_k], E[(x_k - \hat{\mathbf{x}}_k)(x_k - \hat{\mathbf{x}}_k)^T])$$

$$= N(\hat{\mathbf{x}}_k, P_k)$$

(24)

In general, the Kalman filter estimates the process state at time k and then corrects this estimation based on the noisy measurement z_k. The algorithm is based on two sets of equations: *time update* and *measurement update* equations. The time update equations project the current state and error covariance estimates forward in time to obtain the *a priori* estimates for the next time step. On the other hand, the measurement update equations are responsible for the feedback: adding a new measurement into the *a priori* estimate to obtain an improved *a posteriori* estimate.
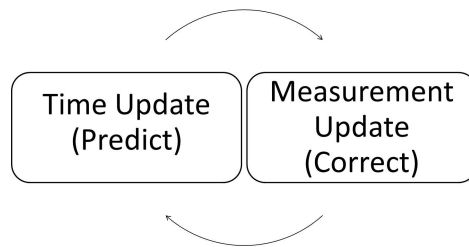
Figure 6: The Ongoing Kalman Filter Cycle

B. Square-Root Cubature Kalman Filters

However, most of the systems that we are dealing with in real life are nonlinear. Thus, research has been intensively conducted in order to find a

nonlinear filtering solution based on the Kalman filter. The research resulted in obtaining the extended Kalman filter, the unscented Kalman filter, and the quadrature Kalman filter. Nevertheless, these filters suffer from divergence or the curse of dimensionality or both.

Recently, Arasaratnam and Haykin derived a more accurate nonlinear filter[12]. This filter can solve high-dimensional nonlinear filtering problems with minimal computational effort. Their work was based on the fact that the Bayesian filter solution in the Gaussian domain reduces to the problem of how to compute multi-dimensional integrals, whose integrands are all of the form nonlinear function ÃŮ Gaussian density. To compute integrals numerically, they derived a third-degree spherical-radial cubature rule. Finally, they combined their cubature rule with the Bayesian filter and created a new filter: The Cubature Kalman Filter (CKF).

The Cubature Kalman filter tries to solve the filtering problem of a dynamic system with additive noise, whose state-space model is defined by the following difference equations:

$$\text{Process Equation: } x_k = f(x_{k-1}, u_{k-1}) + v_{k-1}$$
$$\text{Measurement Equation: } z_k = h(x_k, u_k) + w_k$$

(25)

v_{k-1} and w_k are independent process and measurement Gaussian noise sequences with zero means and covariances Q_{k-1} and R_k respectively. where

$x_k \in \mathbb{R}^{n_x}$ state of the dynamic system at discrete time k

$f : \mathbb{R}^{n_x} \times \mathbb{R}^{n_u} \rightarrow \mathbb{R}^{n_x}$ some known function

$h : \mathbb{R}^{n_x} \times \mathbb{R}^{n_u} \to \mathbb{R}^{n_z}$ some known function

$u_k \in \mathbb{R}^{n_u}$ known control input;

$z_k \in \mathbb{R}^{n_z}$ measurement

v_{k-1} and w_k independent process and measurement Gaussian noise sequences with zero means and covariances Q_{k-1} and R_k respectively.

The cubature rule has many desirable properties that make the CKF an improved algorithm for the nonlinear problems. First, having a state-vector of dimension n requires us to use only $2n$ cubature points. Thus, at each update we are making $2n$ functional evaluations. The computational complexity therefore grows linearly with the dimension n whereas it grows cubically in terms of flops. In other words, the CKF lessens the curse of dimensionality but does not provide a complete solution for this issue. Second, using the CKF with the third-degree cubature rule may be considered as an optimal approximation to the Bayesian filter designed for a nonlinear system, under the Gaussian assumption. Finally, the cubature rule is derivative-free. Therefore, we can apply the CKF to any model with complicated nonlinearities without having to worry about the difficult calculations of the Jacobian and Hessian matrices.

Next, in order to improve numerical stability Arasaratnam and Haykin derived the square-root version of the CKF. The reason behind the SCKF is to maintain the two properties of the error covariance matrix which are symmetry and positive definiteness. Usually these two properties are lost due to errors introduced by arithmetic operations performed on finite word-length digital computers. The CKF algorithm includes matrix square-rooting, matrix inversion

and some other operations that may destroy the properties of the covariance matrix. In addition, some nonlinear filtering problems may be numerically ill which can cause instability and divergence. In order to avoid these problems, they use the SCKF which propagates square-root factors of the predictive and posterior error covariances. It preserves the symmetry and positive semi-definiteness of the covariance and improves numerical accuracy and precision. The SCKF algorithm is based on the least-squares method for the Kalman gain and matrix triangular factorization or triangularization (the QR decomposition) for covariance updates.

As the state dimension n increases, the computational complexity of the SCKF grows cubically in terms of flops . Hence it is comparable to that of the CKF or the EKF. Its complexity can be significantly reduced by taking advantage of the sparsity of the square-root covariance and by using coding triangularization algorithms for distributed processor-memory architectures.

The SCKF algorithm is presented next, where all of the steps can be deduced directly from the CKF except for the update of the posterior error covariance.

Time Update

1) Evaluate the cubature points $(i = 1, 2, ..m)$

$$X_{i,k-1|k-1} = S_{k-1|k-1} \xi_i + \hat{\mathbf{x}}_{k-1|k-1} \tag{26}$$

where $m = 2n_x$

23

2) Evaluate the propagated cubature points $(i = 1, 2, ..m)$

$$X^*_{i,k|k-1} = f(X_{i,k-1|k-1}, u_{k-1}) \tag{27}$$

3) Estimate the predicted state

$$\hat{\mathbf{x}}_{k|k-1} = \frac{1}{m} \sum_{i=1}^{m} X^*_{i,k|k-1} \tag{28}$$

4) Estimate the square-root factor of the predicted error covariance

$$S_{k|k-1} = \mathbf{Tria}([\mathscr{X}^*_{k|k-1} \quad S_{Q,k-1}]) \tag{29}$$

where $S_{Q,k-1}$ denotes a square-root factor of Q_{k-1} such that $Q_{k-1} = S_{Q,k-1}S^T_{Q,k-1}$ and the weighted centered(prior mean is subtracted off) matrix

$$\mathscr{X}^*_{k|k-1} = \frac{1}{\sqrt{m}}[X^*_{1,k|k-1} - \hat{\mathbf{x}}_{k|k-1} \quad X^*_{2,k|k-1} - \hat{\mathbf{x}}_{k|k-1}...X^*_{m,k|k-1} - \hat{\mathbf{x}}_{k|k-1}] \tag{30}$$

Measurement Update

1)Evaluate the cubature points $(i = 1, 2, ..m)$

$$X_{i,k|k-1} = S_{k|k-1}\xi_i + \hat{\mathbf{x}}_{k|k-1} \tag{31}$$

2)Evaluate the propagated cubature points $(i = 1, 2, ..m)$

$$Z_{i,k|k-1} = h(X_{i,k|k-1}, u_k) \tag{32}$$

3)Estimate the predicted measurement

$$\hat{\mathbf{z}}_{k|k-1} = \frac{1}{m} \sum_{i=1}^{m} Z_{i,k|k-1} \tag{33}$$

4)Estimate the square-root of the innovation covariance matrix

$$S_{zz,k|k-1} = \mathbf{Tria}([\mathscr{Z}_{k|k-1}^* \quad S_{R,k}]) \tag{34}$$

where $S_{R,k}$ denotes a square-root factor of R_k such that $R_k = S_{R,k} S_{R,k}^T$ and the weighted centered matrix

$$\mathscr{Z}_{k|k-1} = \frac{1}{\sqrt{m}} [Z_{1,k|k-1} - \hat{\mathbf{z}}_{k|k-1} \quad Z_{2,k|k-1} - \hat{\mathbf{z}}_{k|k-1} ... Z_{m,k|k-1} - \hat{\mathbf{z}}_{k|k-1}] \tag{35}$$

5) Estimate the cross-covariance matrix

$$P_{xz,k|k-1} = \mathscr{X}_{k|k-1} \mathscr{Z}_{k|k-1}^T \tag{36}$$

where the weighted, centered matrix

$$\mathscr{X}_{k|k-1} = \frac{1}{\sqrt{m}} [X_{1,k|k-1} - \hat{\mathbf{x}}_{k|k-1} \quad X_{2,k|k-1} - \hat{\mathbf{x}}_{k|k-1} ... X_{m,k|k-1} - \hat{\mathbf{x}}_{k|k-1}] \tag{37}$$

6)Estimate the Kalman gain

$$W_k = (P_{xz,k|k-1} / S_{zz,k|k-1}^T) / S_{zz,k|k-1} \tag{38}$$

7) Estimate the updated state

$$\hat{\mathbf{x}}_{k|k} = \hat{\mathbf{x}}_{k|k-1} + W_k(z_k - \hat{\mathbf{z}}_{k|k-1}) \tag{39}$$

8) Estimate the square-root factor of the corresponding error covariance

$$S_{k|k} = \textbf{Tria}([\mathscr{X}_{k|k-1} - W_k \mathscr{Z}_{k|k-1} \quad W_k S_{R,k}]) \tag{40}$$

After the forward filtering pass, we ran the backward smoothing pass where it recursively computes the smoothed states and parameters backward in time. The following algorithm for the SCKF forward pass can be found in [13] :

1) Compute the matrices U_{11}, U_{21} and U_{22} using the triangularization algorithm

$$\begin{pmatrix} U_{11} & \mathbf{0} \\ U_{21} & U_{22} \end{pmatrix} = \begin{pmatrix} \mathscr{X}^*_{k+1|k} & S_{Q,k+1} \\ \mathscr{X}_{k|k} & \mathbf{0} \end{pmatrix} \tag{41}$$

where the weighted centered matrix

$$\mathscr{X}_{k|k} = \frac{1}{\sqrt{2n}} \left[X_{1,k/k} - \hat{\mathbf{x}}_{k/k} ... X_{m,k/k} - \hat{\mathbf{x}}_{k/k} \right] \tag{42}$$

2) Compute the smoother gain

$$G_k = U_{21}/U_{11} \tag{43}$$

3) Compute the smoothed state

$$\hat{\mathbf{x}}_{k|N} = \hat{\mathbf{x}}_{k|k} + G_k(\hat{\mathbf{x}}_{k+1|N} - \hat{\mathbf{x}}_{k+1|k}) \tag{44}$$

26

4) Compute the square-root of the smoothed state error covariance

$$S_{k/N} = \textbf{Tria}\left(\begin{bmatrix} U_{22} & G_k S_{k+1/N} \end{bmatrix}\right) \tag{45}$$

CHAPTER IV

MULTI-AREA SEIZURE MODEL UNDER ECT

A. 4-Area Model

Since one block of the Wendling model represents one single area, connecting multiple Wendling blocks will create interaction between neural populations. This will allow one area to initiate a seizure based on the external input and to initiate a feedback excitatory connection with the other areas driving them into seizure activity [6]. The other areas may be driven by inputs that are below seizure-threshold but with the feedback connection will generate a seizure. Hence, the following equations are the updated version of (11) and (13):

$$\dot{x}_e(t) = z_2(t) \tag{46}$$

$$\dot{z}_2(t) = Aa\left[u_0(t) + c_{ep}S\{c_{pe}x_p(t) + k_{p2p1}x_{p2}(t)\}\right] - 2az_2(t) - a^2x_e(t)$$

$$\dot{x}_{if}(t) = z_4(t) \tag{47}$$

$$\dot{z}_4(t) = Ggd_{fp}S\{c_{pf}x_p(t) + k_{p2f1}x_{p2}(t) - d_{sf}x_{ii}(t)\}) - 2gz_4(t) - g^2x_{if}(t)$$

where $x_{p2}(t)$ is the output from the pyramidal cells in area 1 arriving at the other areas. k_{p2p1} and k_{p2f1} are the connections from area 2 to the pyramidal and fast inhibitory cells in area 1, respectively.

Finally, we took into consideration that the signals between areas don't arrive instantly but there is some propagation delay between activity generated in
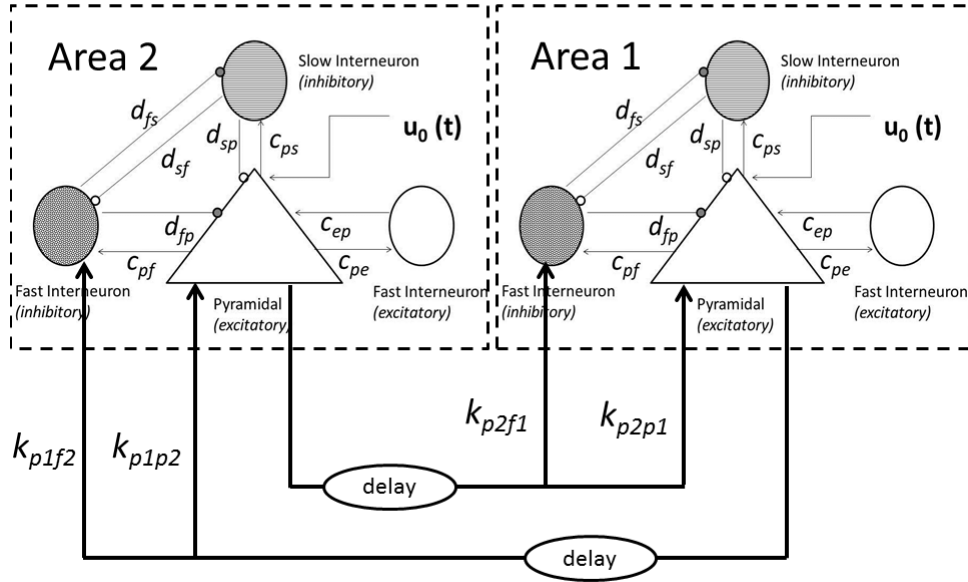
Figure 7: Multi-Area Model

one area and arriving at another. As shown in Figure 7, we added a new function between the connections to account for the delay. Table 1 lists the values of the delays used throughout the simulations where $\tau_{m,n}$ represents the propagation delay between activity generated in area m and arriving at area n :

Delay	Value in (ms)
$\tau_{1,2},\tau_{2,1},\tau_{3,2},\tau_{4,3}$	4
$\tau_{1,3},\tau_{2,4},\tau_{3,1},\tau_{4,2}$	10
$\tau_{1,4},\tau_{2,3},\tau_{3,4},\tau_{4,1}$	8

Table 1: Values of Propagation Delays between different areas

Our final model consists of 4 areas fully connected with each other as shown in Figure 8. Based on the original Wendling model differential equations

29
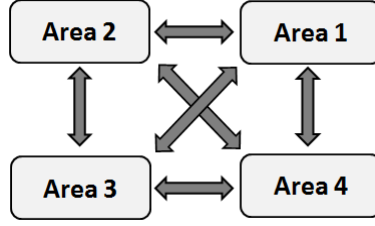
Figure 8: Four Connected Blocks of the Wendling Model

set in addition to the variations made in [6], the 4 areas model consists of 40 differential equations that define the Wendling blocks behavior and the interaction between them. The following set of 10 differential equations represents one area with its local activity and the interaction with the signals arriving from other areas.

$$\dot{x}_p(t) = z_1(t) \tag{48}$$

$$\dot{z}_1(t) = AaS\{x_e(t) - x_{is}(t) - x_{if}(t)\} - 2az_p(t) - a^2x_p(t)$$

$$\dot{x}_e(t) = z_2(t) \tag{49}$$

$$\dot{z}_2(t) = Aa\left[u_0(t) + c_{ep}S\{c_{pe}x_p(t) + k_{p2p1}x_{p2}(t - \tau_{2,1}) + k_{p3p1}x_{p3}(t - \tau_{3,1})\}\right]$$

$$+ k_{p4p1}x_{p4}(t - \tau_{4,1}) - 2az_2(t) - a^2x_e(t)$$

$$\dot{x}_{is}(t) = z_3(t) \tag{50}$$

$$\dot{z}_3(t) = Bbd_{sp}S\{c_{ps}x_p(t) - d_{fs}x_{if}(t)\} - 2bz_3(t) - b^2x_{is}(t)$$

$$\dot{x}_{if}(t) = z_4(t) \tag{51}$$

$$\dot{z}_4(t) = Ggd_{fp}S\{c_{pf}x_p(t) + k_{p2f1}x_{p2}(t - \tau_{2,1}) + k_{p3f1}x_{p3}(t - \tau_{3,1})\})$$

$$+ k_{p4f1}x_{p4}(t - \tau_{4,1}) - d_{sf}x_{ii}(t) - 2gz_4(t) - g^2x_{if}(t)$$

$$\dot{x}_{ii}(t) = z_5(t) \tag{52}$$

$$\dot{z}_5(t) = BbS\{c_{ps}x_p(t)\} - 2bz_5(t) - b^2x_{ii}(t)$$

$$e(t) = K_{iv}\left(x_e(t) - x_{is} - x_{if}(t)\right) \tag{53}$$

Our main goal is to find the values of the connections between brain areas. We will focus on three EEG types : normal EEG activity, ictal and postictal phases. Using the data from the AUB medical center lab, we will run the SCKF in order to find how these parameters are being distributed under the three different cases. Each area is connected to the three other areas by three different connections. In total, We have twelve connection values that we need to find. Basically we want to study how do these connections change in various EEG states. Thus, setting the 12 parameters to certain values will give us a specific EEG signal.

What we are aiming for is different from what Wendling et al did in [5]. They were tuning the internal variables of the Wendling model (A, B and G) in order to get different types of EEG activity. On the other hand, we will fix these internal variables throughout our work to the values found in [5]. We list them in Table 2 on page 34.

Next, we integrated the four Wendling Blocks into the SCKF to create our model. Given the process and measurement equations of the SCKF as:

$$\text{Process Equation: } x_k = f(x_{k-1}, u_{k-1}) + v_{k-1}$$
$$\text{Measurement Equation: } z_k = h(x_k, u_k) + w_k \tag{54}$$

we defined the function f to represent the brain model which is in our case the four connected Wendling blocks. The 40 differential equations that model the four areas have 40 different states. However, three states from each block were

passed to the SCKF which in total gives us 12 states. The 3 states used from each area are $x_e(t), x_{is}(t)$ and x_{if}. As previously mentioned, they are the excitatory input, the GABA$_{\text{A,slow}}$ inhibitory input and the GABA$_{\text{A,fast}}$ inhibitory input, respectively, to the pyramidal cells. The process equation also depends on some input current and the 12 connection parameters. The latter vary according to the SCKF output. On the other hand, the output function h is:

$$e(t) = K_{iv}\left(x_e(t) - x_{is} - x_{if}(t)\right) \tag{55}$$

which calculates the EEG value from three states. Hence, the observed output in SCKF is the four EEG signals corresponding to the four blocks.
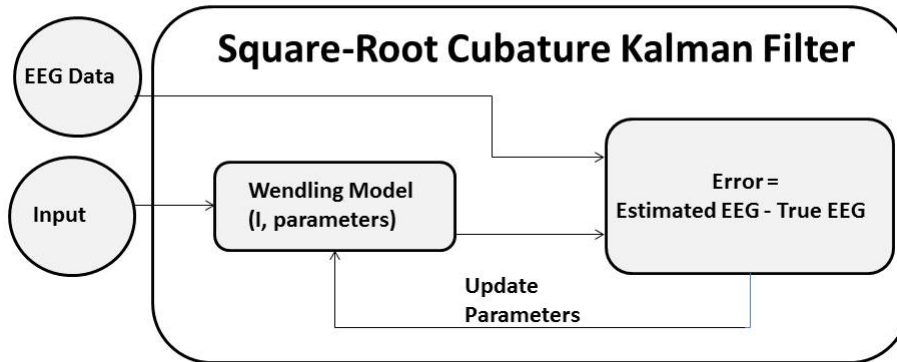
Figure 9: Block Diagram of the Model

In summary, starting with some input current value and an initial estimate of the parameters, the 4 Wendling blocks will generate 4 EEG signals. The SCKF will compare the generated EEG output to the real EEG signals that we want to match. The error difference between the two signals determines how much the parameters will change. The new updated values are fed into the

32

Wendling blocks. The cycle is repeated until the error converges to zero and there is no need to update the parameters anymore. The flow diagram is shown in figure 9.

Finally, we had 12 Wendling states and 12 connection parameter thus n in SCKF is equal to 24 and the number of cubature points m is 48. The Runge-Kutta 4th order method was used to solve the differential equations in Wendling and all the code was written in MATLAB.

Parameter	Interpretation	Standard Value
A	Average excitatory synaptic gain	$3.25mV$
B	Average slow inhibitory synaptic gain	$22mV$
G	Average fast inhibitory synaptic gain	$10mV$
$1/a$	Dendritic average time constant in the feedback excitatory loop	$a = 100s^{-1}$
$1/b$	Dendritic average time constant in the slow feedback inhibitory loop	$b = 50s^{-1}$
$1/g$	Somatic average time constant in the fast feedback inhibitory loop	$g = 500s^{-1}$
C_1, C_2	Average number of synaptic contacts in the excitatory feedback loop	$C_1 = C, C_2 = 0.8C(C = 135)$
C_3, C_4	Average number of synaptic contacts in the slow feedback inhibitory loop	$C_3 = C_4 = 0.25C$
C_5, C_6	Average number of synaptic contacts in the fast feedback inhibitory loop	$C_5 = 0.35C, C_5 = 0.35C$
C_7	Average number of synaptic contacts between slow and fast inhibitory interneurons	$C_7 = 0.8C$
$v_0.e_0, r$	Parameters of the nonlinear asymmetric sigmoid function	$v_0 = 6mV, e_0 = 2.5s^{-1}, r = 0.56mV$

Table 2: Model Parameters Values

B. SCKF Estimation of Connectivity in Surrogate Data

We will show next the results of testing our model on synthetic EEG data. To generate EEG, we ran the 4 Wendling blocks with the internal variables set to the values in Table 2. Then we chose a random combination of the connection parameters as illustrated in Tables 3 and 4.

$k_{p_1p_2}$	$k_{p_1p_3}$	$k_{p_1p_4}$	$k_{p_2p_1}$	$k_{p_2p_3}$	$k_{p_2p_4}$	$k_{p_3p_1}$	$k_{p_3p_2}$	$k_{p_3p_4}$	$k_{p_4p_1}$	$k_{p_4p_2}$	$k_{p_4p_3}$
60	10	15	20	30	10	30	12	16	43	50	6

Table 3: Values of Parameters

$k_{p_1f_2}$	$k_{p_1f_3}$	$k_{p_1f_4}$	$k_{p_2f_1}$	$k_{p_2f_3}$	$k_{p_2f_4}$	$k_{p_3f_1}$	$k_{p_3f_2}$	$k_{p_3f_4}$	$k_{p_4f_1}$	$k_{p_4f_2}$	$k_{p_4f_3}$
30	5	7.5	10	15	5	15	6	8	21.5	25	3

Table 4: Values of Parameters

The four inputs of the model $u_1(t), u_2(t), u_3(t)$ and $u_4(t)$ arriving at areas $1, 2, 3$ and 4 respectively are shown in Figure 10a. By setting the parameters and the inputs to the mentioned values, we generated the EEG synthetic output shown in Figure 10b. Next, we fed this synthetic data to the SCKF as our desired output and we ran it for 4 seconds. The goal was to test whether the SCKF can fit the true EEG data and find the right set of parameters. As displayed in Figure 10c, the SCKF was able to track the generated model data with high accuracy by predicting the proper values of parameters for the network. The absolute error is plotted in Figure 10d. Figures 11(a),11(b) and 11(c) show that the SCKF converges also to the right set of parameters that we used in the model. Moreover looking at the Wendling states of the system, we find that the SCKF is also able to produce all 12 correct states as displayed in Figures 11(d), 11(e) and 11(f). Based on these results, we can conclude that our

(a) Input $u(t)$

(b) EEG Model Output Signal

(c) Overlapping Synthetic Data and SCKF
Output Data
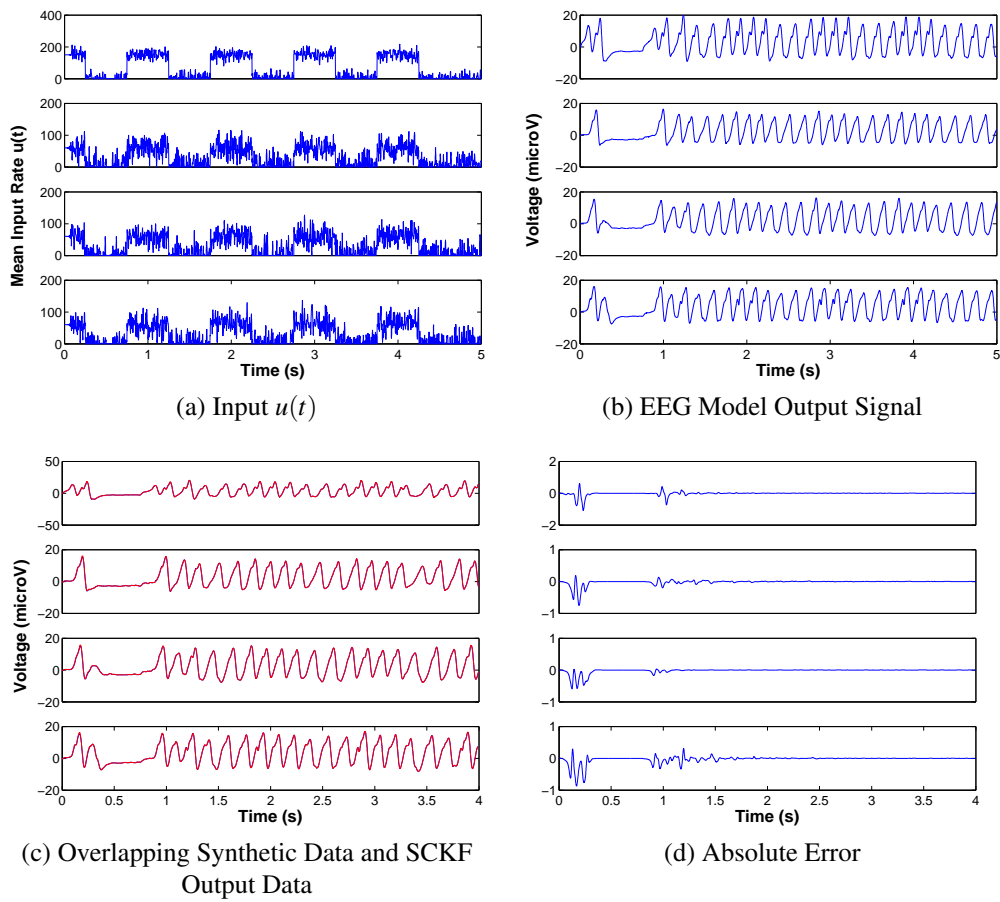
(d) Absolute Error

Figure 10: Surrogate Data Results: Input and Output Signals, Absolute Error

model can track the correct EEG output while converging to the right set of parameters and thus the true states of the system.
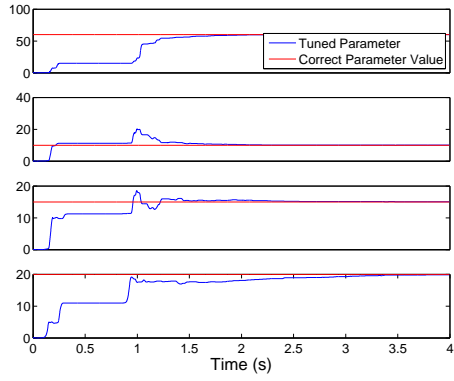
(a) Parameters $k_{p_1 p_2}$, $k_{p_1 p_3}$, $k_{p_1 p_4}$, $k_{p_2 p_1}$
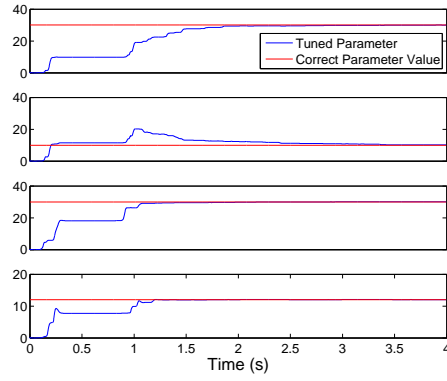
(b) Parameters $k_{p_2 p_3}$, $k_{p_2 p_4}$, $k_{p_3 p_1}$, $k_{p_3 p_2}$
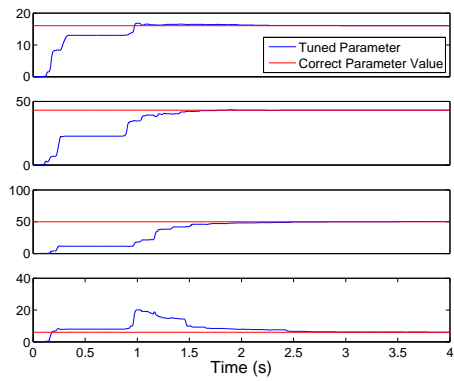
(c) Parameters $k_{p_3 p_4}$, $k_{p_4 p_1}$, $k_{p_4 p_2}$, $k_{p_4 p_3}$
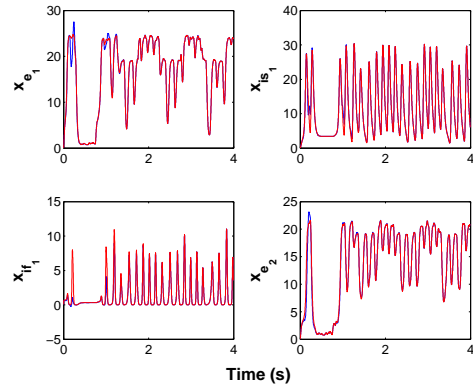
(d) States $x_{e_1}, x_{is_1}, x_{if_1}, x_{e_2}$
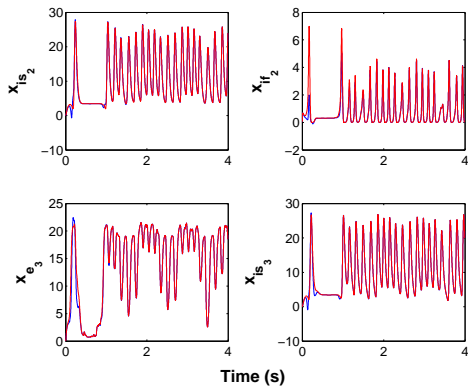
(e) states $x_{is_2}, x_{if_2}, x_{e_3}, x_{is_3}$
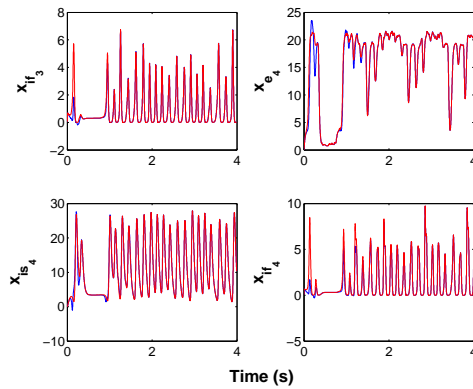
(f) states $x_{if_3}, x_{e_4}, x_{is_4}, x_{if_4}$

Figure 11: Surrogate Data Results: Parameters and States

CHAPTER V

RESULTS

In this chapter, we will show the results of testing our model on real EEG data from the lab. As explained in the previous chapter, our model consists of four interconnected areas and our goal is to find the values of the connection parameters. There are three types of EEG signals that we used through our work: i) normal ii) ictal and iii) postictal states. We aim to find the difference in the distribution of parameters for the different EEG states.

A. Data Set

We have been provided with ECT data for five subjects form the AUBMC (Dr Ziad Nahas, IRB approved protocols). The data set consists of ECT recorded sessions for five different subjects. Each subject has 0 or 1 recorded titration session and 2 recorded treatment sessions as illustrated in Table 5.

Subject Number	Number of Titration Sessions	Number of Treatment Sessions	Reverse Polarity
1	1	2	×
2	0	2	×
3	1	2	Treatment 1
4	1	2	Treatment 2
5	0	2	Treatment 1

Table 5: subject Data distribution

During the ECT session, the electrodes are placed on the scalp according to the FEAST(focal electrically administered seizure therapy) configuration. This method combines unidirectional stimulation, control of polarity, and an asymmetrical electrode configuration (small anterior and large posterior electrode). FEAST is based on the hypothesis that by improving the focality of the treatment we may lessen its side effects without affecting the antidepressant efficacy [1].

B. Additional Smoothing

Each session was divided into three parts: normal, ictal and postictal. Each part consists of 10 seconds of EEG data scaled down by a factor of 2. As discussed earlier our goal is to find the values of the parameters for each state. We had two setups for the different states:

- In the normal and postictal states, we ran the SCKF first as the forward run and then we ran the square-root cubature Kalman smoother as the backward run in order to smooth the values of parameters. We assigned a vector of zeros as initial values for the parameters and the model was able to converge to a certain set of values for the normal and postictal states.

- In the ictal state, we also ran the SCKF first as a forward run and then we ran the square-root cubature Kalman smoother as the backward run. However, the values of parameters were excessively fluctuating thus we added a third step that consists of taking the average value of the resulting parameter and using it as an initial value for a second run (forward and

39

backward again). The result was a much more smoothed parameter value for the ictal state.

C. Global Areas

First, we study the parameter modeling for global areas to model relative activity of remote areas in the brain. For the global areas, the four brain areas are taken to be the EEG signals recorded by electrodes $F6, F5, P5$ and $P4$ which are found in the frontal and parietal lobes respectively. Figure 12 shows the position of the electrodes and Table 6 lists the four areas with their corresponding electrodes.

Area	Electrode
1	F6
2	F5
3	P5
4	P4

Table 6: Electrodes in different areas

The connection parameters are displayed in Figure 13. Table 7 lists the different parameters and their corresponding connected areas. In the next section, the parameters $k_{p_1 p_2}, k_{p_1 p_3}, k_{p_1 p_4}, k_{p_2 p_1}, k_{p_2 p_3}, k_{p_2 p_4}, k_{p_3 p_1}, k_{p_3 p_2}, k_{p_3 p_4}, k_{p_4 p_1}, k_{p_4 p_2}$ and $k_{p_4 p_3}$ will be referred to as $P1$, $P2$, $P3$, $P4$, $P5$, $P6$, $P7$, $P8$, $P9$, $P10$, $P11$ and $P12$ respectively.
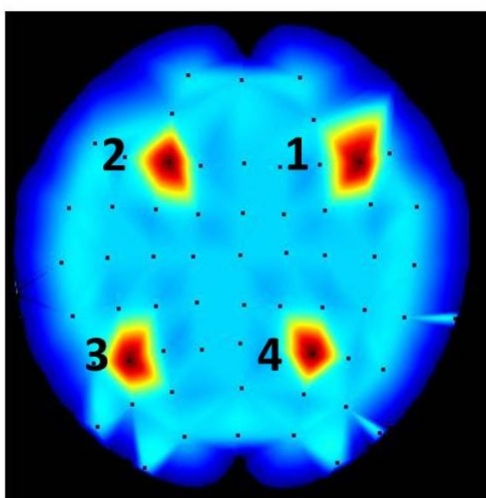
Figure 12: The 4 brain areas

	Area 1	Area 2	Area 3	Area 4
Area 1		$k_{p_1 p_2}$	$k_{p_1 p_3}$	$k_{p_1 p_4}$
Area 2	$k_{p_2 p_1}$		$k_{p_2 p_3}$	$k_{p_2 p_4}$
Area 3	$k_{p_3 p_1}$	$k_{p_3 p_2}$		$k_{p_3 p_4}$
Area 4	$k_{p_4 p_1}$	$k_{p_4 p_2}$	$k_{p_4 p_3}$	

Table 7: The connection parameters between the four areas
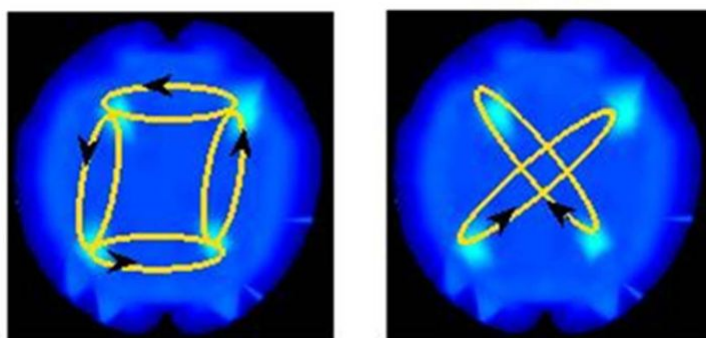
Figure 13: The 12 parameters

41
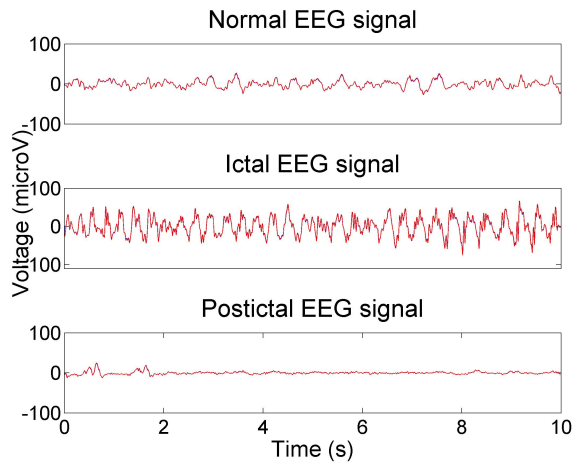
Figure 14: Subject 3. Treatment 1: EEG Data and SCKF Output Data of normal, ictal and postictal states

D. SKCF Modeling and Accuracy for Global Areas

We ran SKCF for the different EEG signals obtained from the subjects in table 5. The resultant models were highly accurate. For illustration, we will show the detailed results of the first treatment session for subject number 3. As mentioned earlier, we want the SCKF to be able to track the true EEG signal and to find the values of parameters. Figure 14 shows the EEG data and the SCKF output data of the normal, ictal and postictal states. The output of the SCKF is clearly overlapping the true EEG signal. Figure 15 and 16 show the convergence of the 12 parameters for the normal and postictal smoothed values are also shown in 15 and 16 as the green line plot for the normal and postictal states respectively. Similarly, Figure 17 shows the convergence of the 12 parameters for the ictal state with their smoothed values corresponding to the first run. Finally, Figure 18 shows the convergence of the 12 parameters for the ictal state with their smoothed values after the second run of the SCKF.

(a) Parameters $k_{p_1p_2}$, $k_{p_1p_3}$, $k_{p_1p_4}$

(b) Parameters $k_{p_2p_1}$, $k_{p_2p_3}$, $k_{p_2p_4}$

(c) Parameters $k_{p_3p_1}$, $k_{p_3p_2}$, $k_{p_3p_4}$

(d) Parameters $k_{p_4p_1}$, $k_{p_4p_2}$, $k_{p_4p_3}$
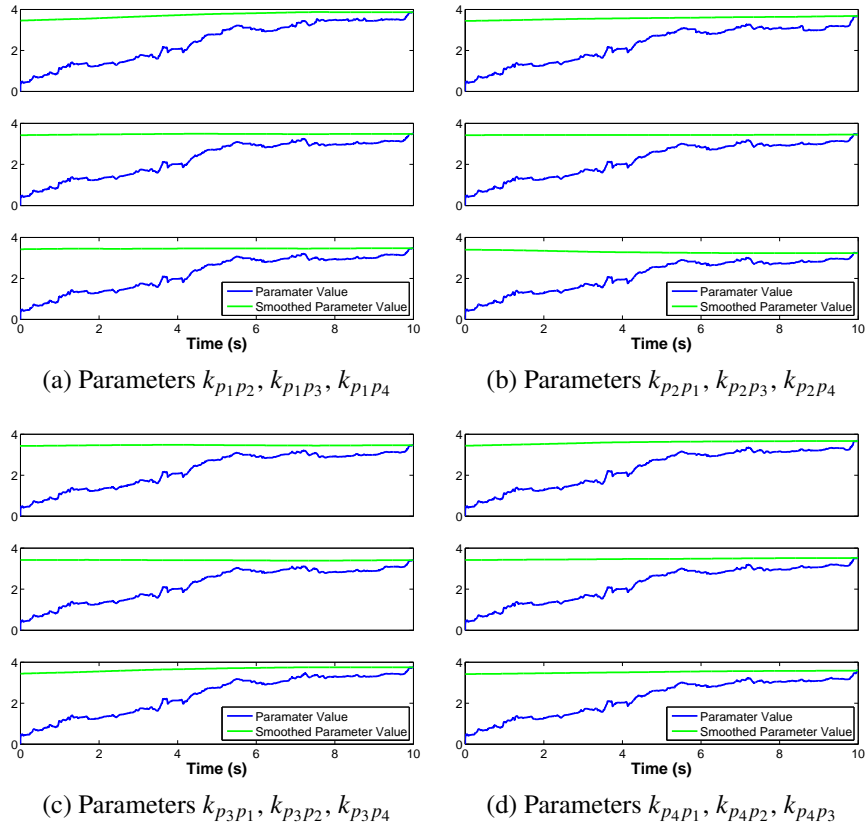
Figure 15: Subject 3, Treatment 1: Values of Unsmoothed and Smoothed Parameters for the Normal State

(a) Parameters $k_{p_1p_2}$, $k_{p_1p_3}$, $k_{p_1p_4}$

(b) Parameters $k_{p_2p_1}$, $k_{p_2p_3}$, $k_{p_2p_4}$

(c) Parameters $k_{p_3p_1}$, $k_{p_3p_2}$, $k_{p_3p_4}$

(d) Parameters $k_{p_4p_1}$, $k_{p_4p_2}$, $k_{p_4p_3}$
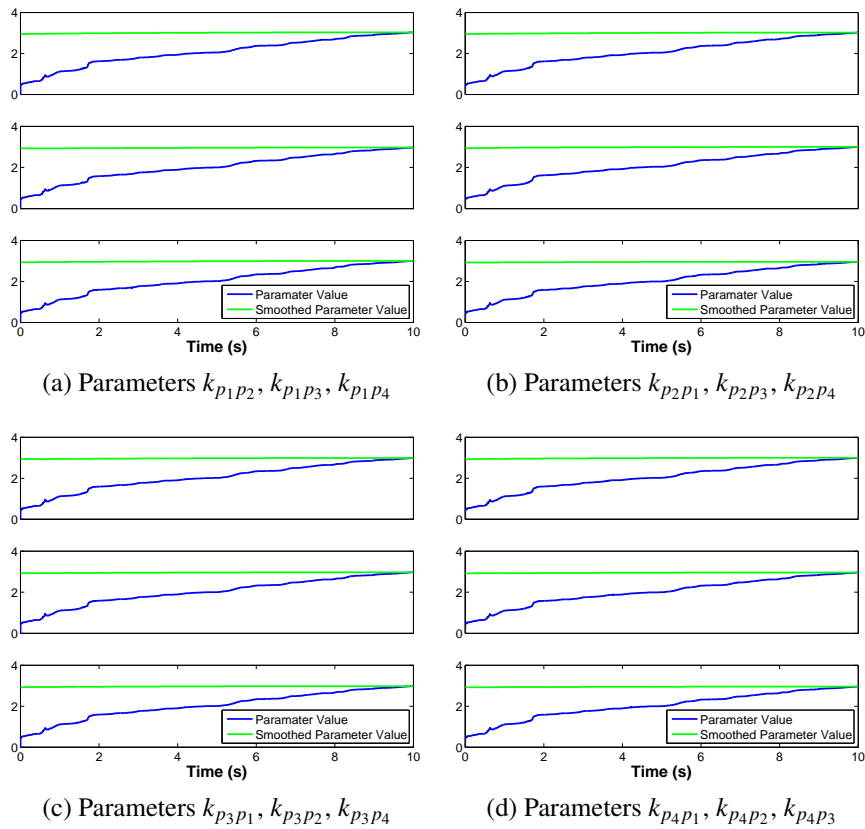
Figure 16: Subject 3, Treatment 1: Values of Unsmoothed and Smoothed Parameters for the Postictal State

(a) Parameters $k_{p_1p_2}$, $k_{p_1p_3}$, $k_{p_1p_4}$

(b) Parameters $k_{p_2p_1}$, $k_{p_2p_3}$, $k_{p_2p_4}$

(c) Parameters $k_{p_3p_1}$, $k_{p_3p_2}$, $k_{p_3p_4}$

(d) Parameters $k_{p_4p_1}$, $k_{p_4p_2}$, $k_{p_4p_3}$
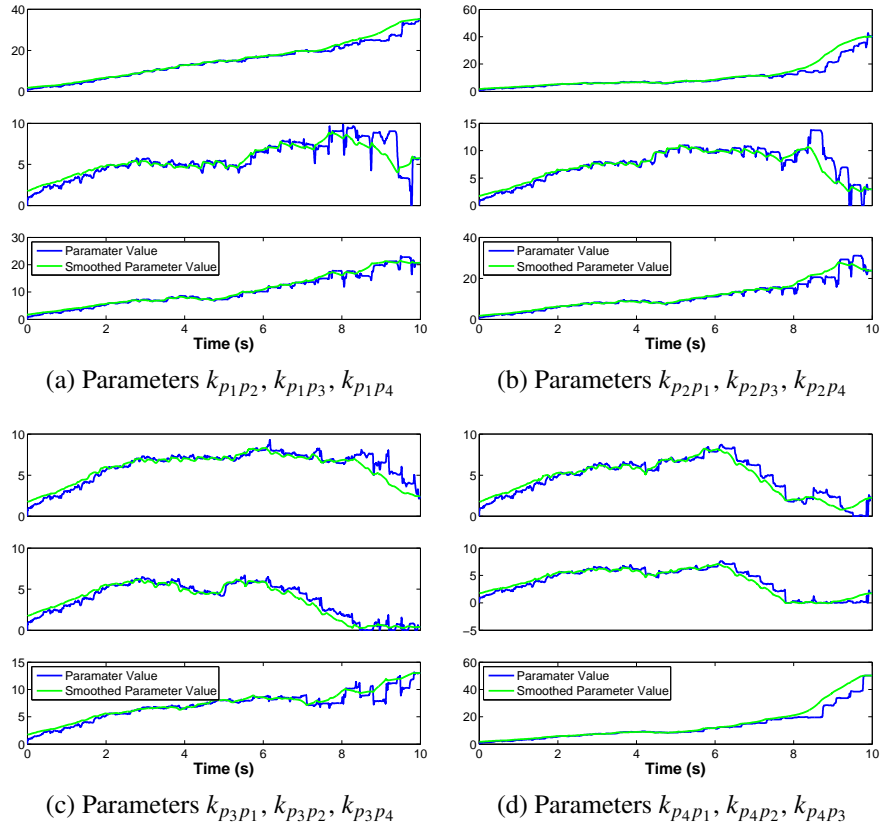
Figure 17: Subject 3, Treatment 1: Values of Unsmoothed and Smoothed Parameters for the Ictal State , First Run

(a) Parameters $k_{p_1p_2}$, $k_{p_1p_3}$, $k_{p_1p_4}$

(b) Parameters $k_{p_2p_1}$, $k_{p_2p_3}$, $k_{p_2p_4}$

(c) Parameters $k_{p_3p_1}$, $k_{p_3p_2}$, $k_{p_3p_4}$

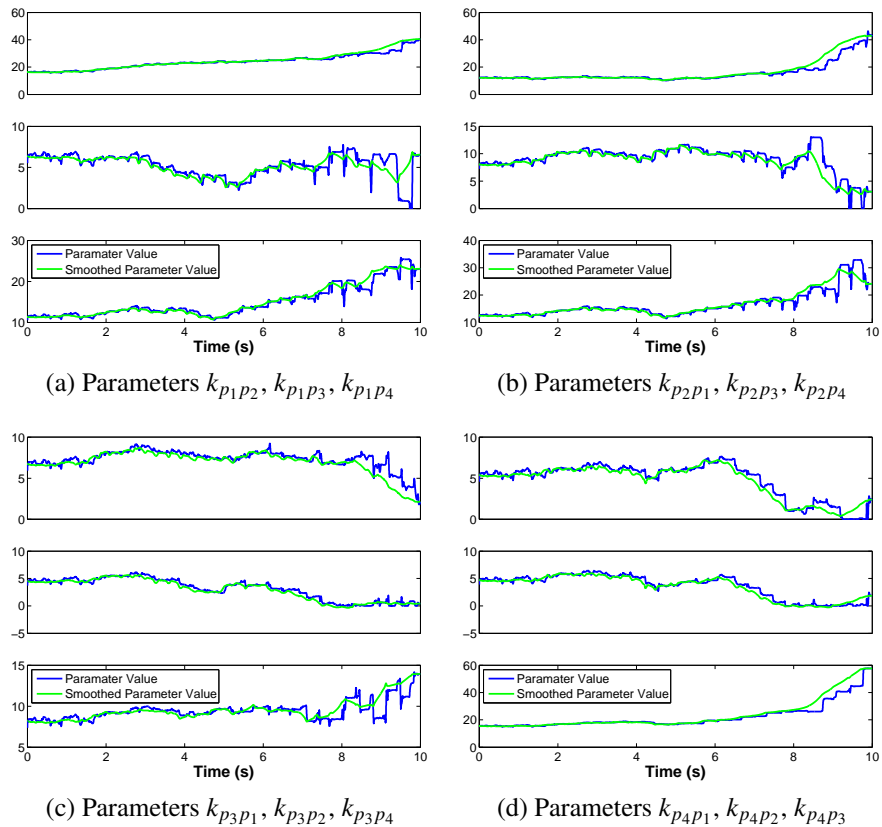(d) Parameters $k_{p_4p_1}$, $k_{p_4p_2}$, $k_{p_4p_3}$

Figure 18: Subject 3, Treatment 1: Values of Unsmoothed and Smoothed Parameters for the Ictal State, Second Run

E. Critical Study of Parameter Distribution- Global Areas

As was illustrated in the figures, the parameters in the seizure state have higher values than those in the normal and postictal states. Thus, to critically analyze this difference, we calculate the change in seizure and postictal parameters with respect to the normal ones for all sessions according to the following equations

$$\Delta_i = \frac{\mathbf{p}_{ictal} - \mathbf{p}_{normal}}{\mathbf{p}_{normal}} \tag{56}$$

$$\Delta_p = \frac{\mathbf{p}_{postictal} - \mathbf{p}_{normal}}{\mathbf{p}_{normal}} \tag{57}$$

where $\mathbf{p}_{normal}, \mathbf{p}_{ictal}$ and $\mathbf{p}_{postictal}$ are the parameters in the normal, ictal and postictal states respectively.

In what follows, we present the corresponding statistics for each subject. Each subject section includes the following figures:

1. EEG signal in normal, ictal and postictal states

2. A boxplot that summarizes the values of the 12 parameters

3. A boxplot that summarizes the change in the values of the 12 parameters Δ_i and Δ_p relative to the normal state as explained in (56) and (57)

4. A bar plot that displays the average power signal in the four areas during the three different EEG states to understand the different signals strength.

5. A table showing the maximum, minimum, mean and standard deviation values of Δ_i and Δ_p across all parameters

1. Subject 1

The following is a summary for the data of the first subject. Tables 8 and 9 show the statistics of the normalized change in parameters during the ictal and postictal states respectively. Each row of the table tabulate the maximum value, minimum value, mean and standard deviation of all 12 parameters of the corresponding ECT session. Figures 19, 21 and 23 display the values of the 12 parameters during the titration, treatment 1 and 2 sessions respectively. Figure 20 shows the EEG power in different states across the 4 areas during the titration session. it also portrays the values of the normalized change in parameters Δ_i and Δ_p. Figure 22 and 24 display the same information but for treatment 1 and treatment 2 sessions.

	Max	Min	Mean	Std
Titration	129.8056	-9.108	10.41722	9.398436
Treatment 1*	16.98419	-0.73097	6.235382	3.076956
Treatment 2	23.37058	-0.71729	4.962609	3.384356

Table 8: Subject 1: Statistics of normalized change in parameter Δ_s during the postictal state, *Reversed polarity

	Max	Min	Mean	Std Dev
Titration	-0.54253	-0.7303	-0.62666	0.032475
Treatment 1*	-0.20218	-0.68205	-0.48662	0.106325
Treatment 2	-0.55546	-0.68034	-0.62638	0.028131

Table 9: Subject 1: Statistics of normalized change in parameter Δ_p during the postictal state, *Reversed polarity
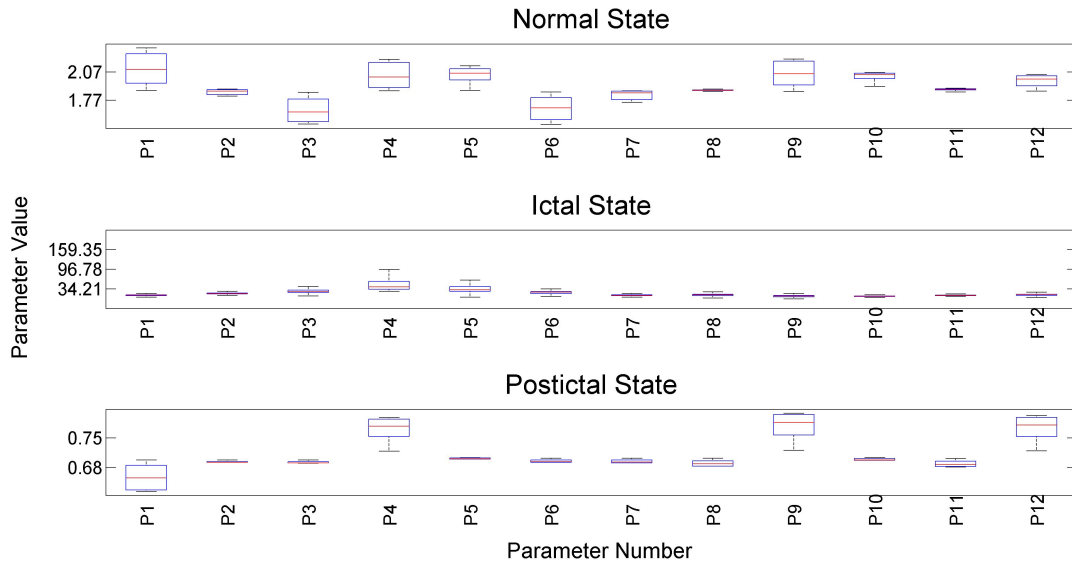
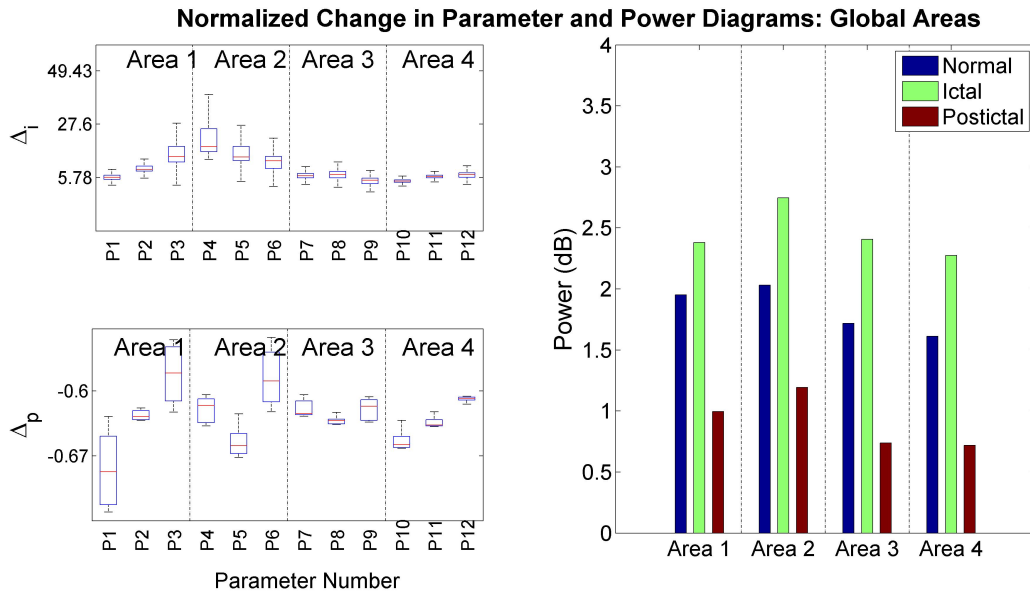Figure 19: Subject 1, Titration 1: Values of Parameters during the three various EEG states

Figure 20: Subject 1, Titration 1: Normalized change in parameter indicates low activity correlation in the postictal state and high activity correlation in the ictal state between the areas; Power diagrams show high power in the ictal state and low power in the postictal state

Figure 21: Subject 1, Treatment 1: Values of Parameters during the three various EEG states

Figure 22: Subject 1, Treatment 1: Normalized change in parameter indicates low activity correlation in the postictal state and high activity correlation in the ictal state between the areas; Power diagrams show high power in the ictal state and low power in the postictal state
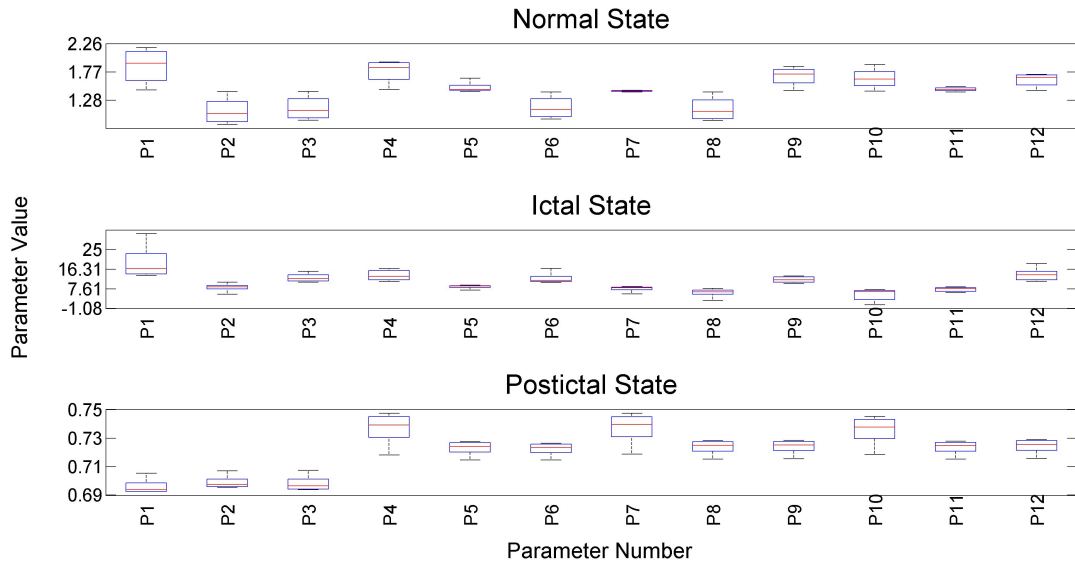
Figure 23: Subject 1, Treatment 2: Values of Parameters during the three various EEG states
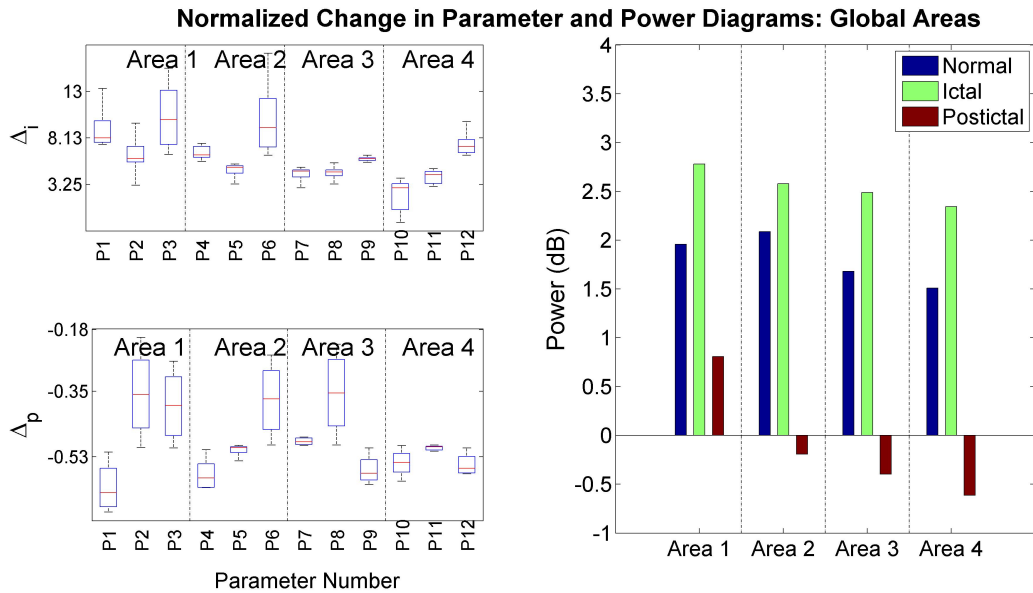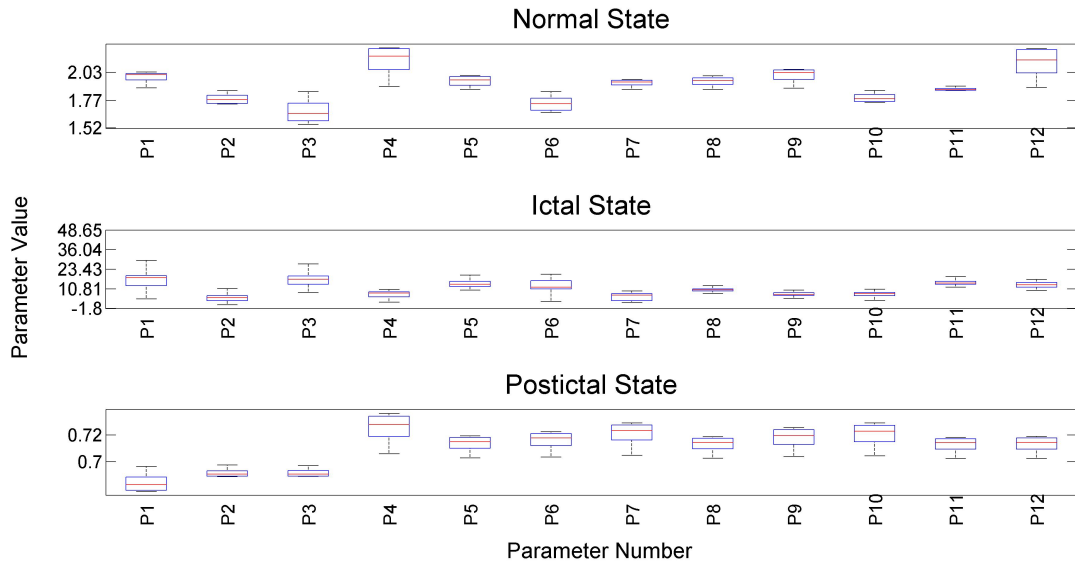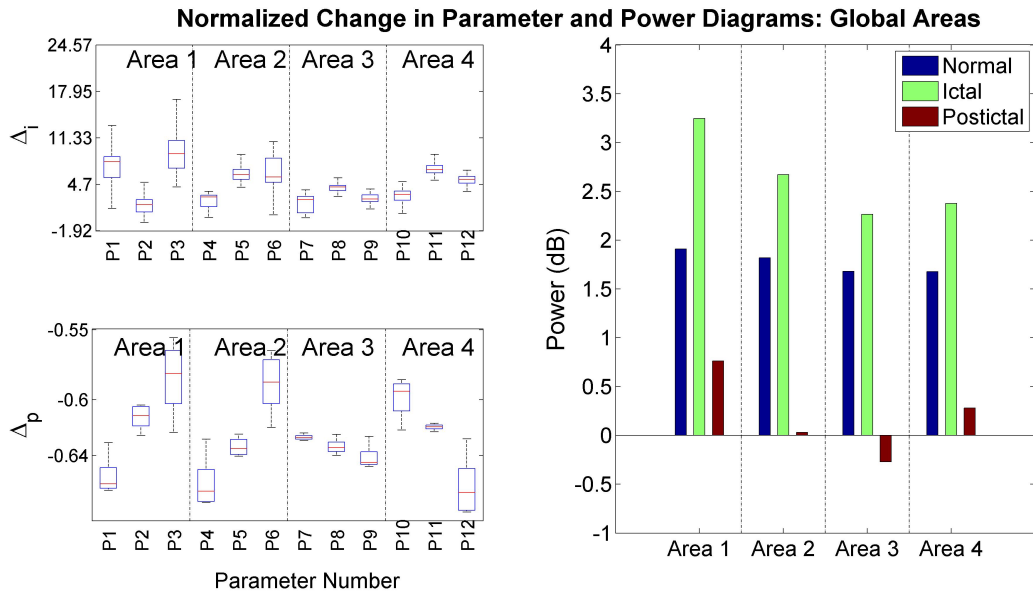

Figure 24: Subject 1, Treatment 2: Normalized change in parameter indicates low activity correlation in the postictal state and high activity correlation in the ictal state between the areas; Power diagrams show high power in the ictal state and low power in the postictal state

2. *Subject 2*

The following is a summary for the data of the second subject. Tables 10 and 11 show the statistics of the normalized change in parameters during the ictal and postictal states respectively. Each row of the table tabulate the maximum value, minimum value, mean and standard deviation of all 12 parameters of the corresponding ECT session. Figures 25 and 27 display the values of the 12 parameters during treatment 1 and 2 sessions respectively. Figure 26 shows the EEG power in different states across the 4 areas during treatment 1 session. it also portrays the values of the normalized change in parameters Δ_i and Δ_p. Figure 28 displays the same information but for treatment treatment 2 session.

		Max	Min	Mean	Std Dev
Subject 2	Treatment 1	7.198436	0.111749	3.574245	1.249382
	Treatment 2	0.765245	0.343096	0.596251	0.06432

Table 10: Subject 2: Statistics of normalized change in parameter Δ_s during the postictal state

		Max	Min	Mean	Std Dev
Subject 2	Treatment 1	0.038793	-0.1205	-0.03878	0.030192
	Treatment 2	-0.42431	-0.5506	-0.45623	0.025809

Table 11: Subject 2: Statistics of normalized change in parameter Δ_p during the postictal state

50

Figure 25: Subject 2, Treatment 1: Values of Parameters during the three various EEG states

Figure 26: Subject 2, Treatment 1: Normalized change in parameter indicates low activity correlation in the postictal state and high activity correlation in the ictal state between the areas; Power diagrams show high power in the ictal state and low power in the postictal state
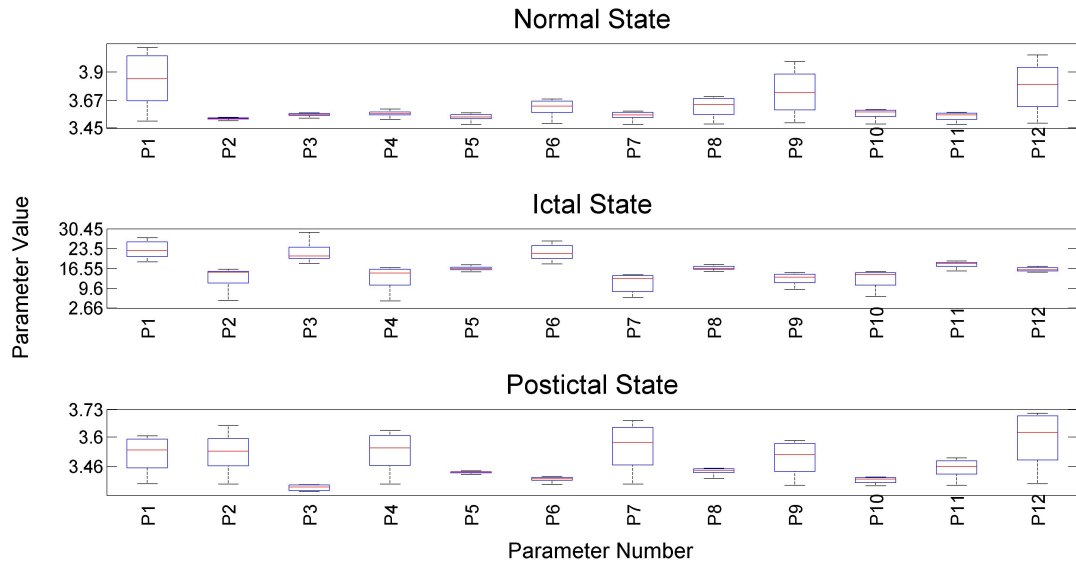
Figure 27: Subject 2, Treatment 1: Values of Parameters during the three various EEG states
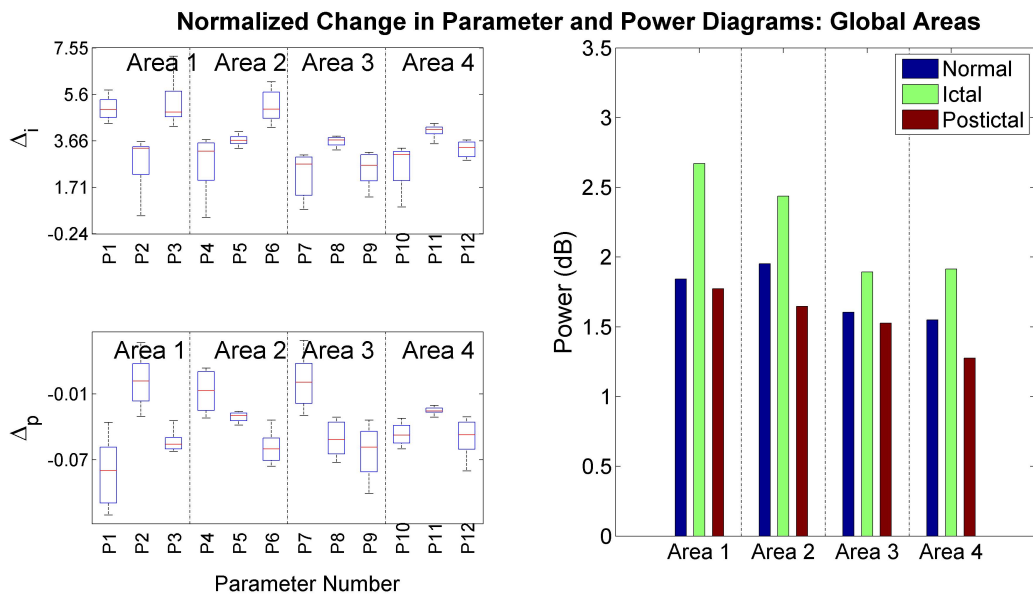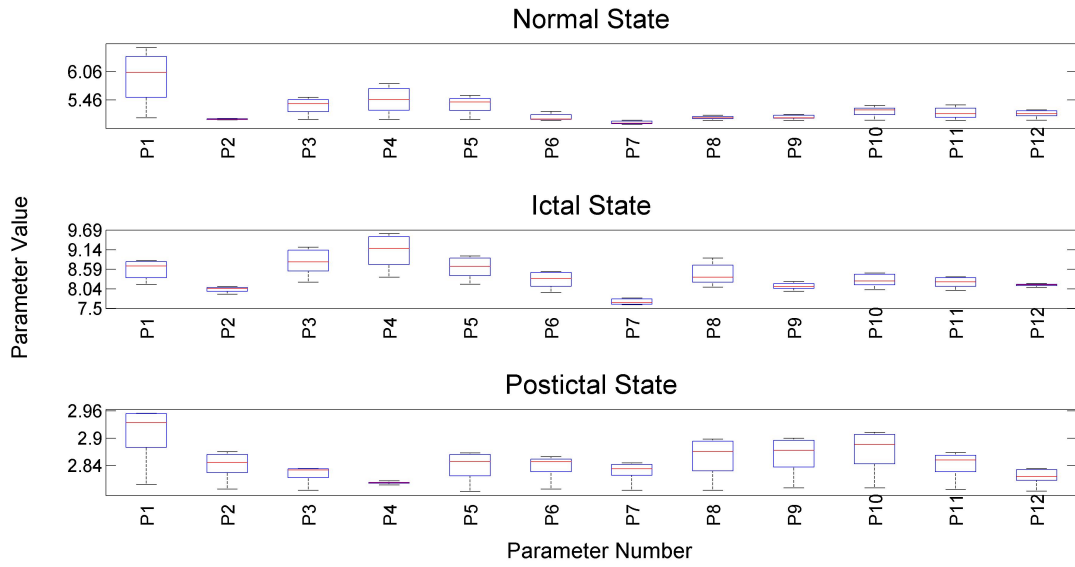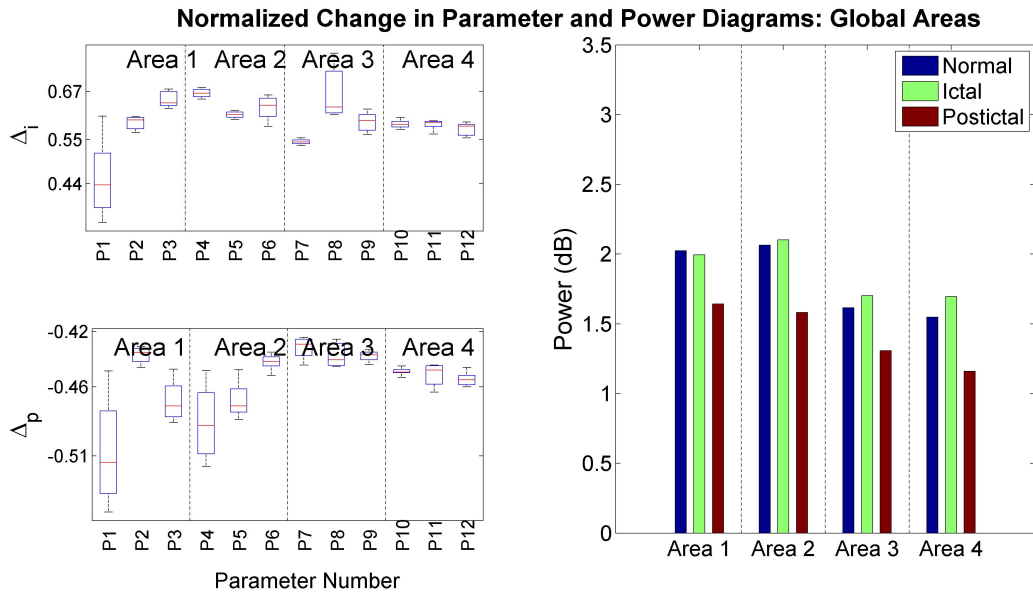

Figure 28: Subject 2, Treatment 1: Normalized change in parameter indicates low activity correlation in the postictal state and high activity correlation in the ictal state between the areas; Power diagrams show high power in the ictal state and low power in the postictal state

3. Subject 3

The following is a summary for the data of the third subject. Tables 12 and 13 show the statistics of the normalized change in parameters during the ictal and postictal states respectively. Each row of the table tabulate the maximum value, minimum value, mean and standard deviation of all 12 parameters of the corresponding ECT session. Figures 29, 31 and 33 display the values of the 12 parameters during the titration, treatment 1 and 2 sessions respectively. Figure 30 shows the EEG power in different states across the 4 areas during the titration session. it also portrays the values of the normalized change in parameters Δ_i and Δ_p. Figure 32 and 34 display the same information but for treatment 1 and treatment 2 sessions.

	Max	Min	Mean	Std Dev
Titration	11.50666	-1.05852	2.718602	2.676634
Treatment 1	15.06745	-1.10959	2.250154	2.435741
Treatment 2	22.28275	-1.87734	2.567572	2.7007

Table 12: Subject 3: Statistics of normalized change in parameter Δ_s during the postictal state

	Max	Min	Mean	Std Dev
Titration	-0.37395	-0.48513	-0.42502	0.023956
Treatment 1	-0.08445	-0.21786	-0.15188	0.027282
Treatment 2	-0.97904	-0.99257	-0.98472	0.00345

Table 13: Subject 3: Statistics of normalized change in parameter Δ_p during the postictal state
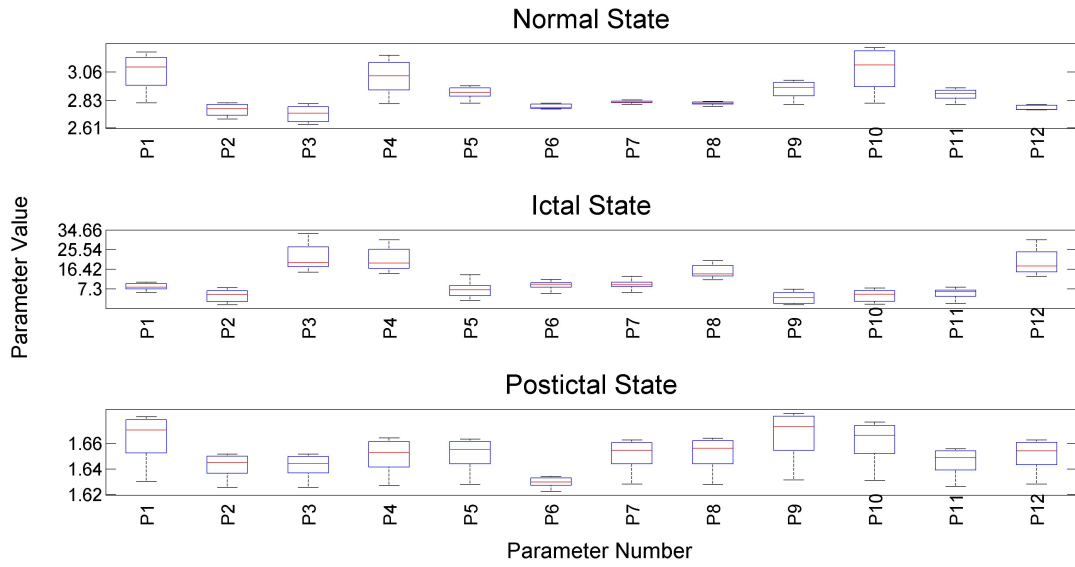
Figure 29: Subject 3, Titration 1: Values of Parameters during the three various EEG states

Figure 30: Subject 3, Titration 1: Normalized change in parameter indicates low activity correlation in the postictal state and high activity correlation in the ictal state between the areas; Power diagrams show high power in the ictal state and low power in the postictal state

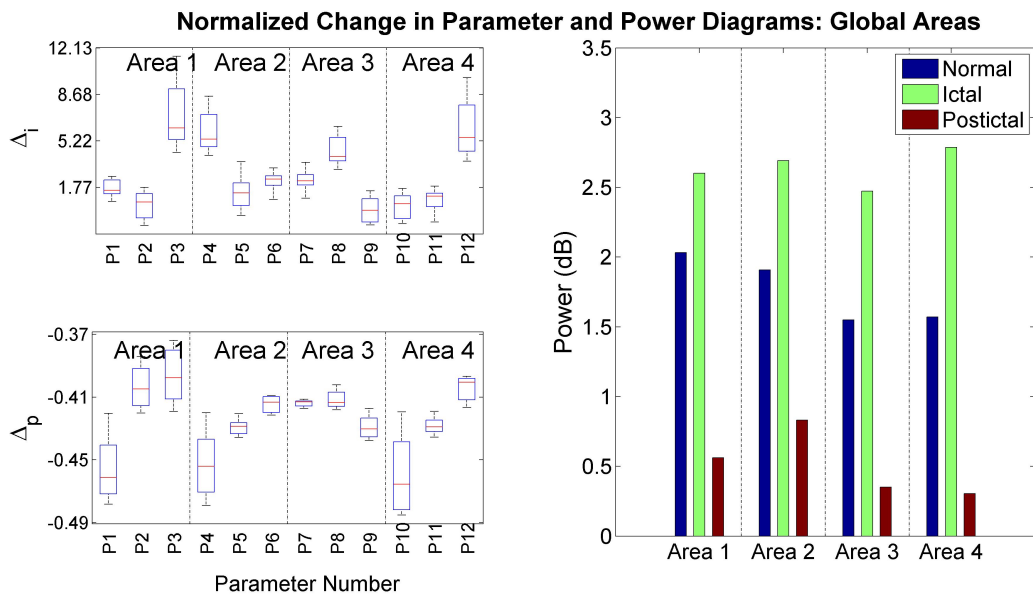Figure 31: Subject 3, Treatment 1: Values of Parameters during the three various EEG states

Figure 32: Subject 3, Treatment 1: Normalized change in parameter indicates low activity correlation in the postictal state and high activity correlation in the ictal state between the areas; Power diagrams show high power in the ictal state and low power in the postictal state
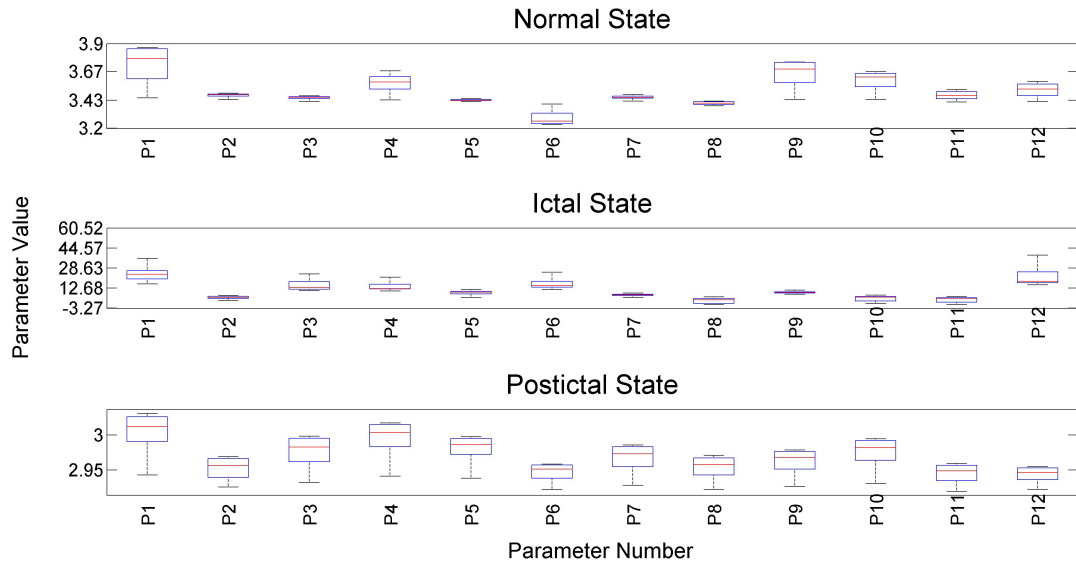
Figure 33: Subject 3, Treatment 2: Values of Parameters during the three various EEG states
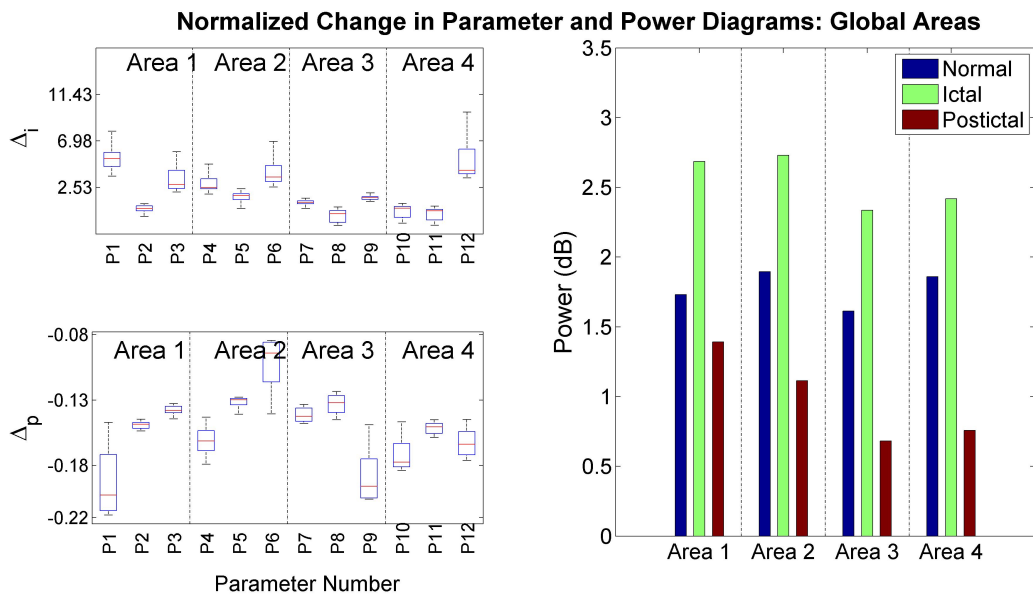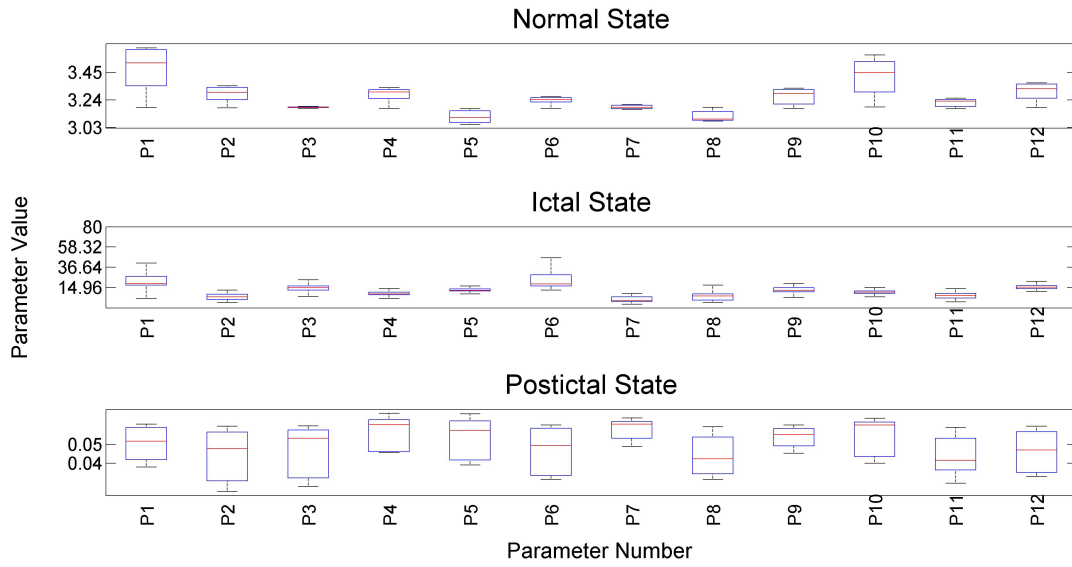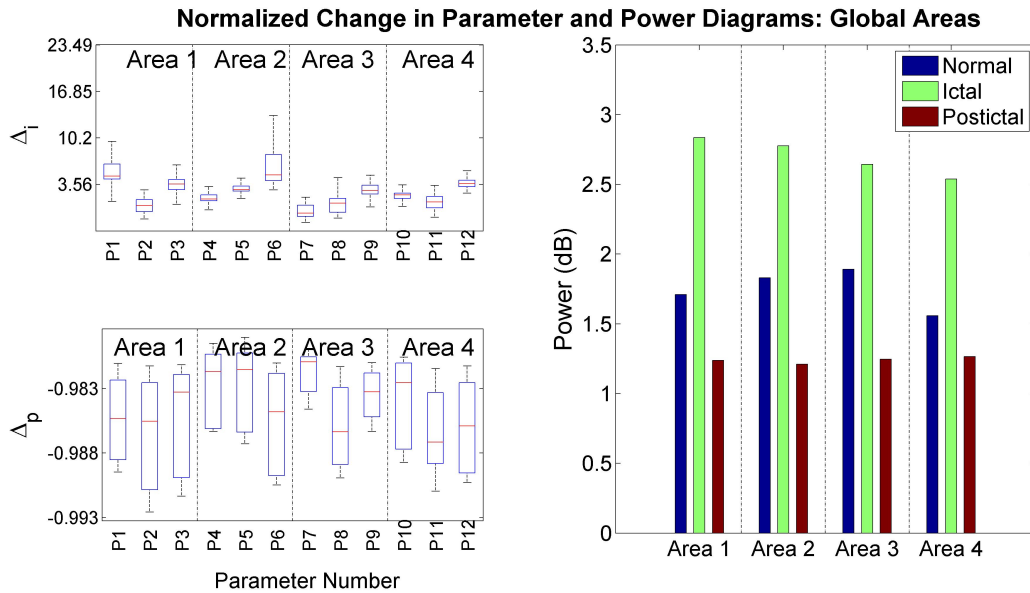

Figure 34: Subject 3, Treatment 2: Normalized change in parameter indicates low activity correlation in the postictal state and high activity correlation in the ictal state between the areas; Power diagrams show high power in the ictal state and low power in the postictal state

4. Subject 4

The following is a summary for the data of the fourth subject. Tables 14 and 15 show the statistics of the normalized change in parameters during the ictal and postictal states respectively. Each row of the table tabulate the maximum value, minimum value, mean and standard deviation of all 12 parameters of the corresponding ECT session. Figures 35, 37 and 39 display the values of the 12 parameters during the titration, treatment 1 and 2 sessions respectively. Figure 36 shows the EEG power in different states across the 4 areas during the titration session. it also portrays the values of the normalized change in parameters Δ_i and Δ_p. Figure 38 and 40 display the same information but for treatment 1 and treatment 2 sessions.

		Max	Min	Mean	Std Dev
	Titration	2.638187	1.409651	1.820667	0.281372
Subject 4	Treatment 1	5.238391	-0.8633	1.037261	0.769766
	Treatment 2*	7.46162	0.810648	2.320972	1.080637

Table 14: Subject 4: Statistics of normalized change in parameter Δ_s during the postictal state, *Reversed polarity

		Max	Min	Mean	Std Dev
	Titration	0.601388	0.242833	0.420236	0.063795
Subject 4	Treatment 1	-0.88365	-0.91863	-0.89967	0.007219
	Treatment 2*	-0.42292	-0.52017	-0.46149	0.019505

Table 15: Subject 4: Statistics of normalized change in parameter Δ_p during the postictal state, *Reversed polarity
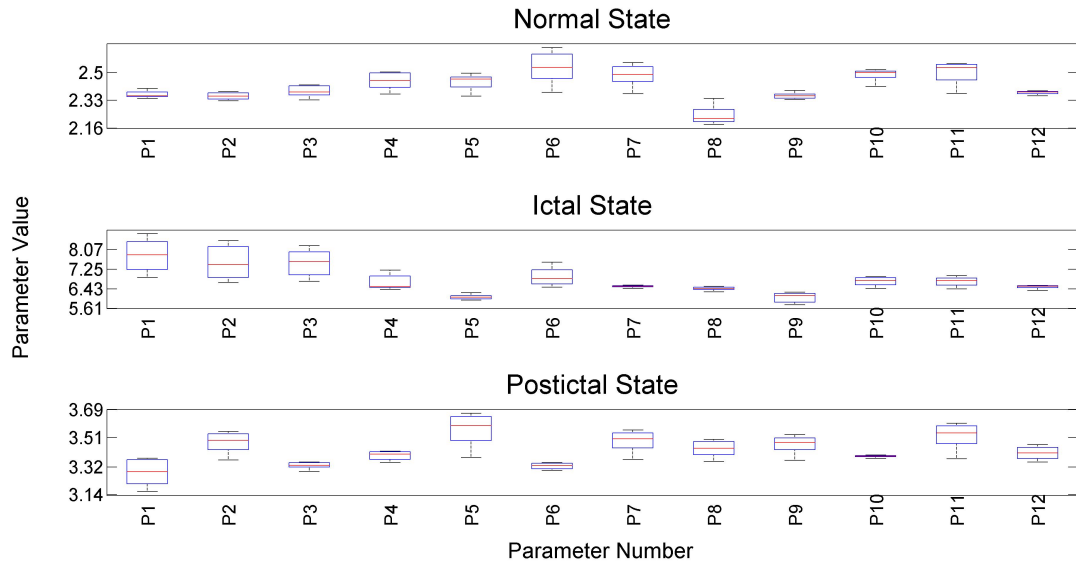
Figure 35: Subject 4, Titration 1: Values of Parameters during the three various EEG states

Figure 36: Subject 4, Titration 1: Normalized change in parameter indicates low activity correlation in the postictal state and high activity correlation in the ictal state between the areas; Power diagrams show high power in the ictal state and low power in the postictal state

Figure 37: Subject 4, Treatment 1: Values of Parameters during the three various EEG states
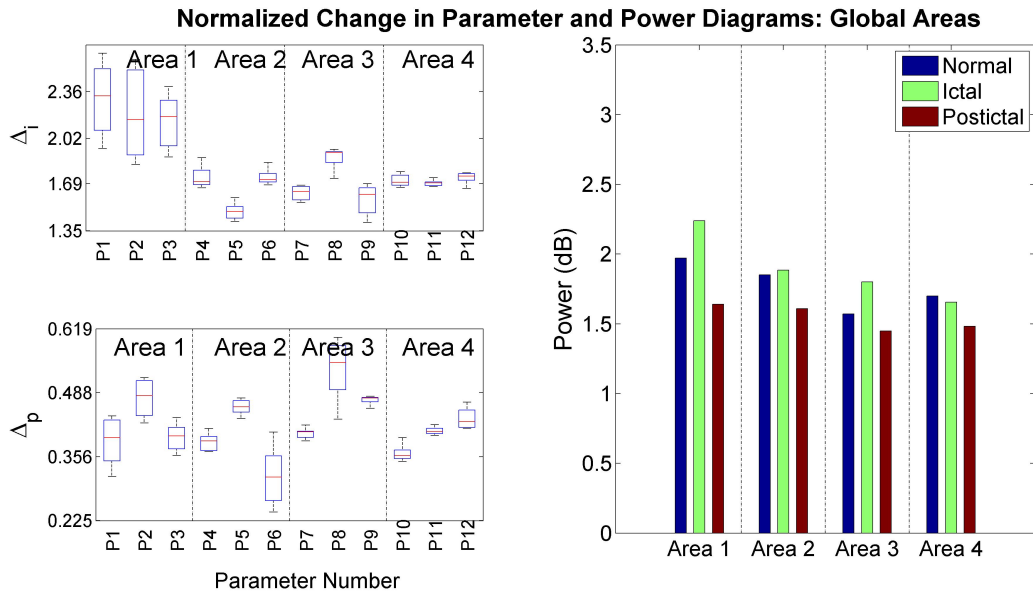

Figure 38: Subject 4, Treatment 1: Normalized change in parameter indicates low activity correlation in the postictal state and high activity correlation in the ictal state between the areas; Power diagrams show high power in the ictal state and low power in the postictal state

Figure 39: Subject 4, Treatment 2: Values of Parameters during the three various EEG states

Figure 40: Subject 4, Treatment 2: Normalized change in parameter indicates low activity correlation in the postictal state and high activity correlation in the ictal state between the areas; Power diagrams show high power in the ictal state and low power in the postictal state
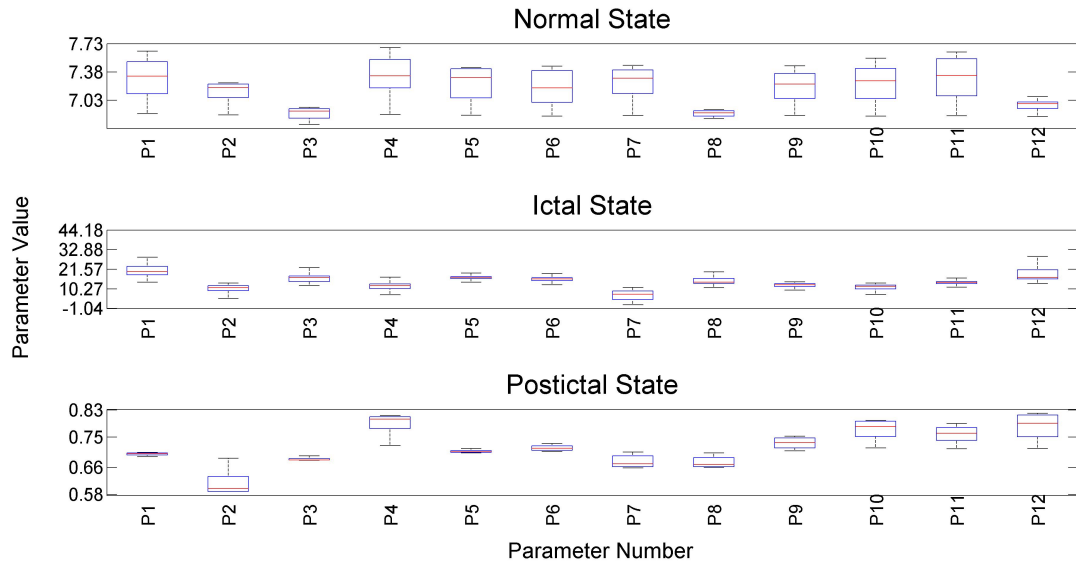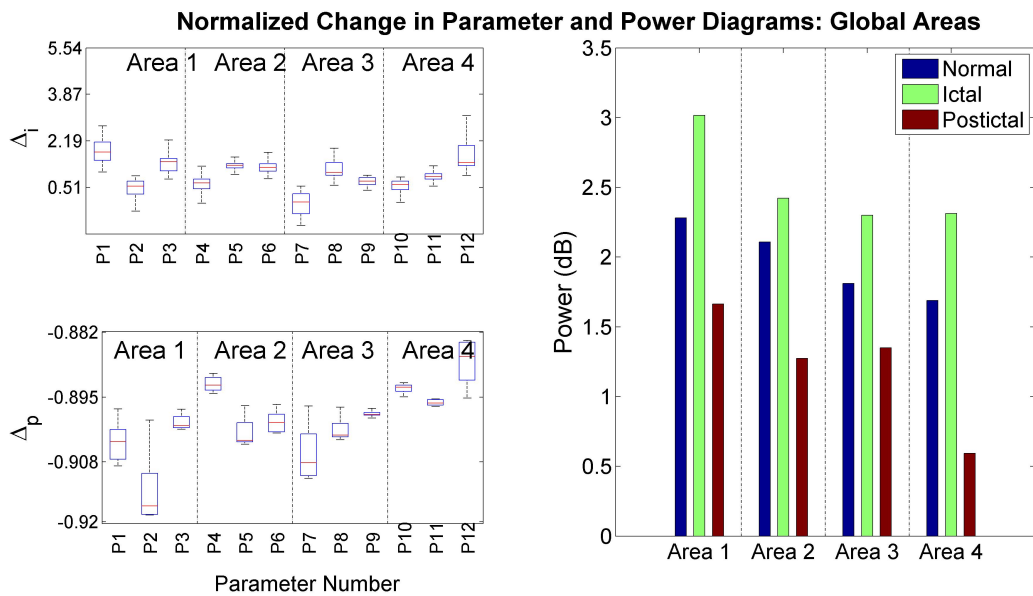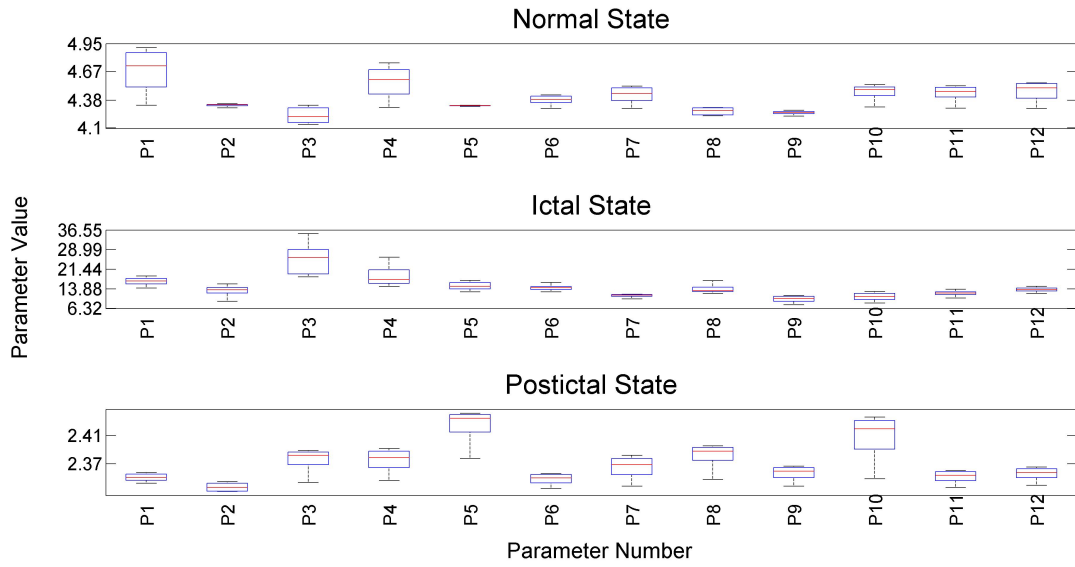
5. *Subject 5*

The following is a summary for the data of the fifth subject. Tables 16 and 17 show the statistics of the normalized change in parameters during the ictal and postictal states respectively. Each row of the table tabulate the maximum value, minimum value, mean and standard deviation of all 12 parameters of the corresponding ECT session. Figures **??** and 41 display the values of the 12 parameters during treatment 1 and 2 sessions respectively. Figure **??** shows the EEG power in different states across the 4 areas during treatment 1 session. it also portrays the values of the normalized change in parameters Δ_i and Δ_p. Figure 42 displays the same information but for treatment treatment 2 session.

		Max	Min	Mean	Std Dev
Subject 5	Treatment 1*	9.086039	1.381543	3.997328	1.088005
	Treatment 2	59.38175	-3.82689	3.691253	4.442815

Table 16: Subject 5: Statistics of normalized change in parameter Δ_s during the postictal state, *Reversed polarity

		Max	Min	Mean	Std Dev
Subject 5	Treatment 1*	0.237762	-0.0362	0.118692	0.054397
	Treatment 2	-0.53661	-0.65161	-0.58619	0.025335

Table 17: Subject 5: Statistics of normalized change in parameter Δ_p during the postictal state, *Reversed polarity

Figure 41: Subject 5, Treatment 1: Values of Parameters during the three various EEG states

Figure 42: Subject 5, Treatment 1: Normalized change in parameter indicates low activity correlation in the postictal state and high activity correlation in the ictal state between the areas; Power diagrams show high power in the ictal state and low power in the postictal state

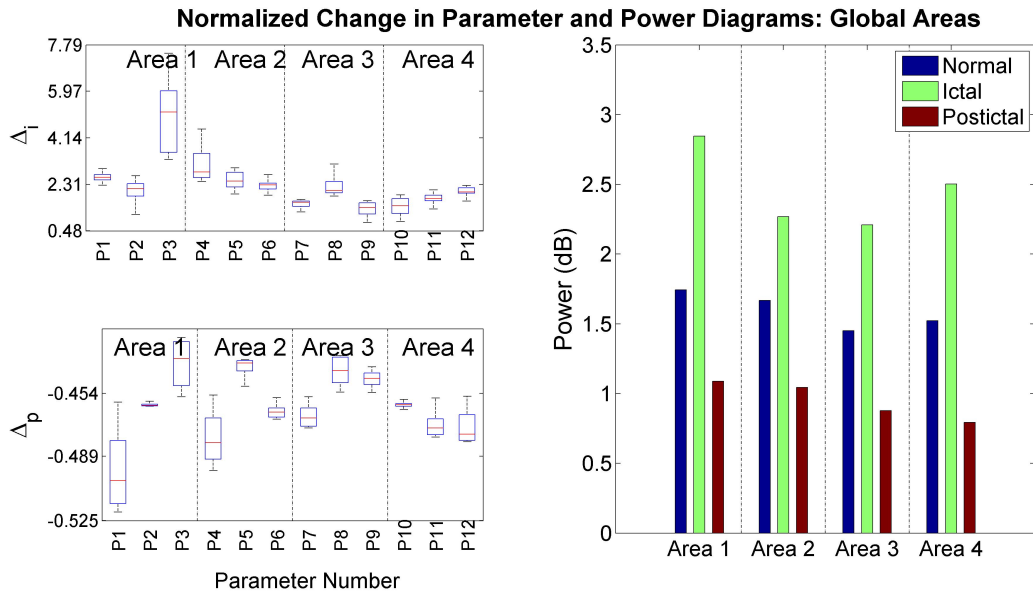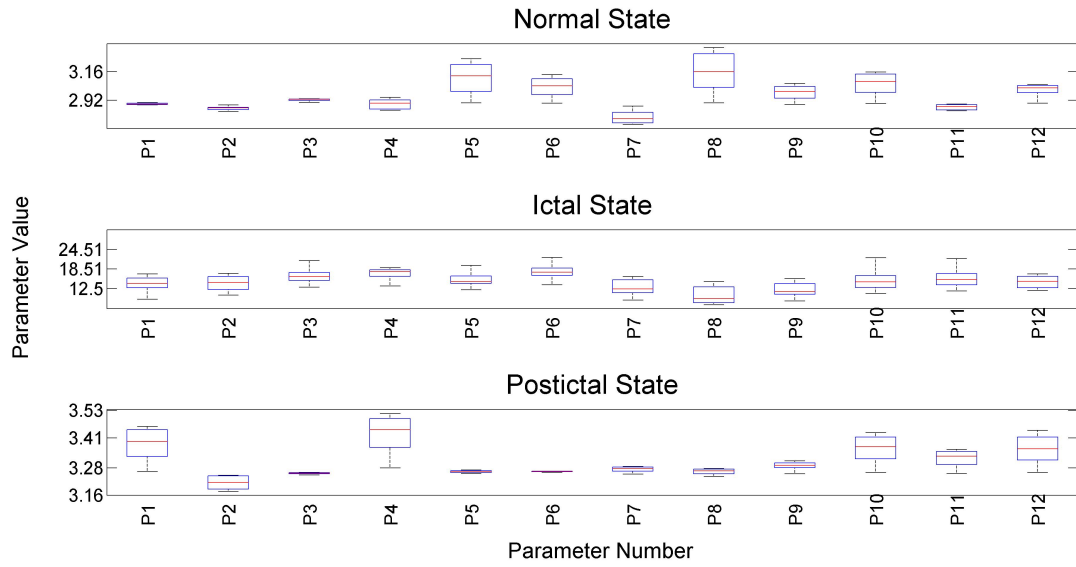Figure 43: Subject 5, Treatment 2: Values of Parameters during the three various EEG states
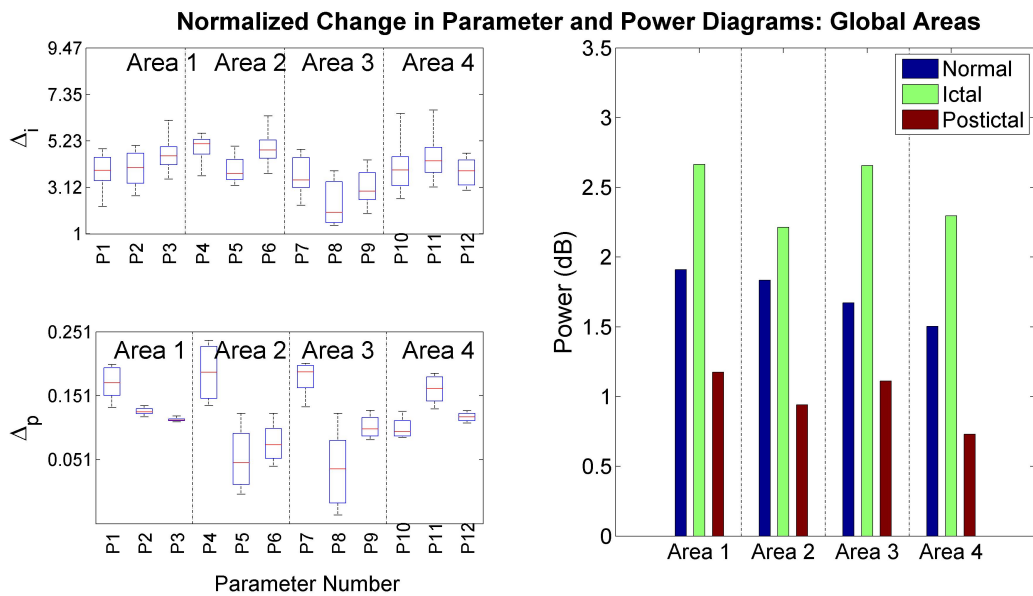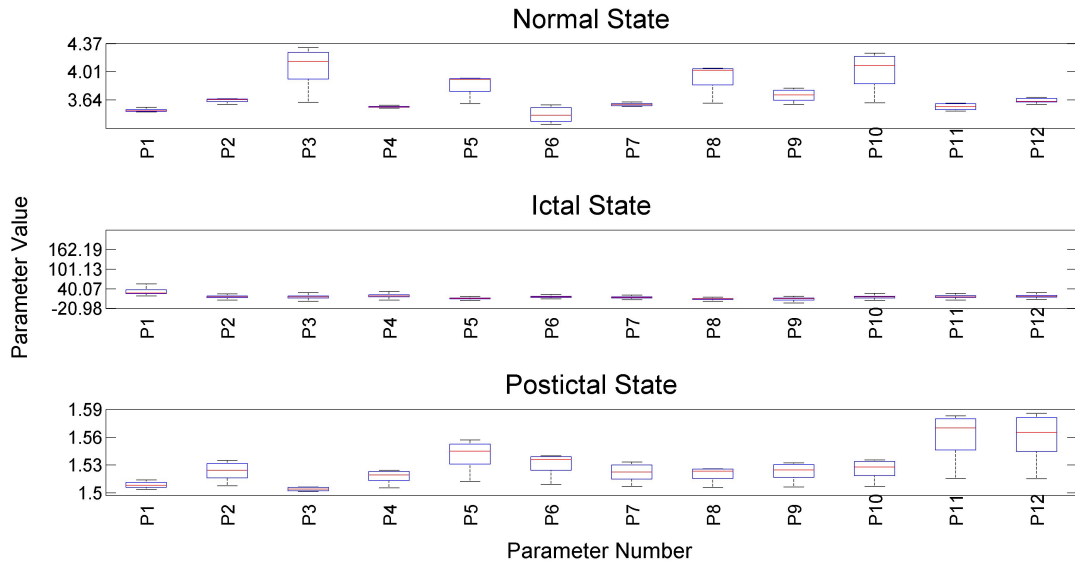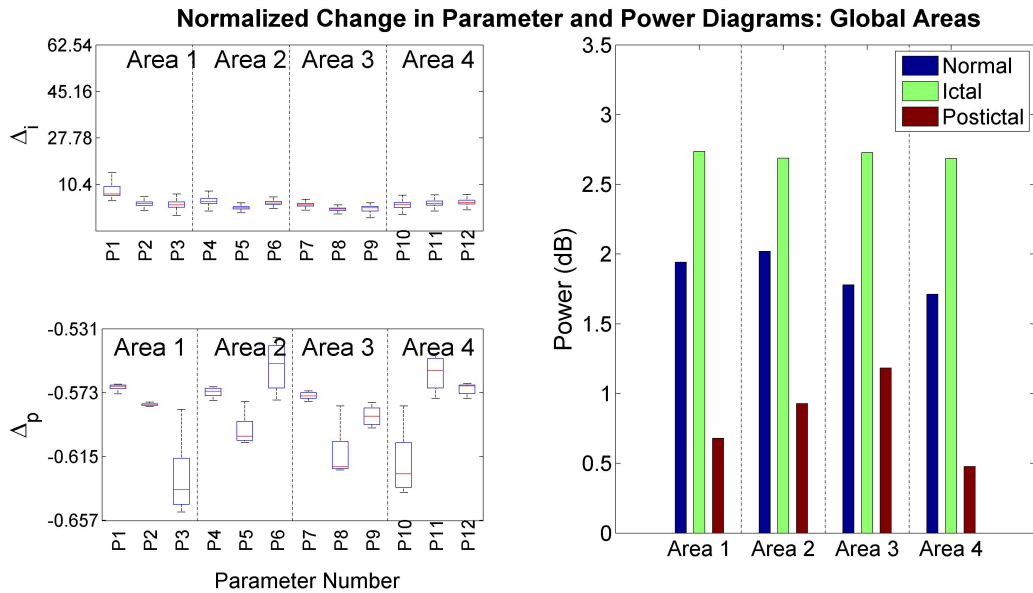

Figure 44: Subject 5, Treatment 2: Normalized change in parameter indicates low activity correlation in the postictal state and high activity correlation in the ictal state between the areas; Power diagrams show high power in the ictal state and low power in the postictal state

F. Local Areas

In order to study the parameter distribution and the activity of local areas, we tested the model on different brain areas as shown in Figure 45. Tables 18 and 19 list the electrodes recording the EEG signals in the right and left frontal areas and the right and left parietal areas respectively.

Local Area 1: Right Frontal		Local Area 2: Left Frontal	
Area	Electrode	Area	Electrode
1	F4	1	F5
2	F6	2	F3
3	FC4	3	FC5
4	FC6	4	FC3

Table 18: Electrodes used for the right and left frontal areas

Local Area 3: Right Parietal		Local Area 4: Left Parietal	
Area	Electrode	Area	Electrode
1	P4	1	P3
2	P6	2	P5
3	PO4	3	PO3
4	PO6	4	PO5

Table 19: Electrodes used for the right and left parietal areas

The results are shown for subject 3. Tables 20 and 21 show the statistics of the normalized change in parameters for the frontal and parietal regions during the ictal and postictal states respectively. Each row of the table tabulate the maximum value, minimum value, mean and standard deviation of all 12 parameters of the corresponding ECT session. Figures 46 and 54 display the values of the 12 parameters for the right frontal region during treatment 1 and 2 sessions respectively. Figure 47 shows the EEG power in different states across
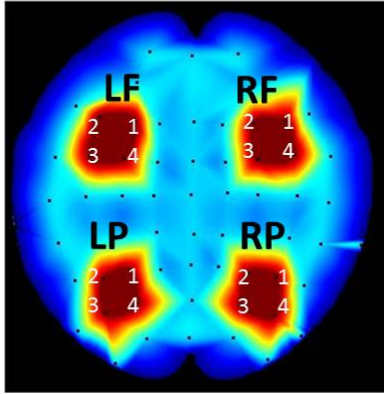
64

Figure 45: Local Brain Areas

the 4 areas in the right frontal region during treatment 1 session. it also portrays the values of the normalized change in parameters Δ_i and Δ_p. Figure 55 displays the same information but for treatment 2 session. Similarly we have the values of the parameters for the left frontal, right and left parietal regions during treatment 1 in Figures 48, 50 and 52 and during treatment 2 in Figures 56, 58 and 60 respectively. In addition, Figures 49, 51 and 53 display the EEG power and the change in parameters for the left frontal, right and left parietal regions during treatment 1 while 57, 59 and 61 display this info during treatment 2. Tables 20 and 21 show the statistics of the normalized change in parameters during the ictal and postictal states respectively for the frontal and parietal regions. Each row of the table tabulate the maximum value, minimum value, mean and standard deviation of all 12 parameters of the corresponding ECT session.

As noticed in the global areas, we also notice that the parameters in the

seizure state have higher values than those in the normal and postictal states. In addition, the parameters in the postictal state have lower values than those in the normal state.
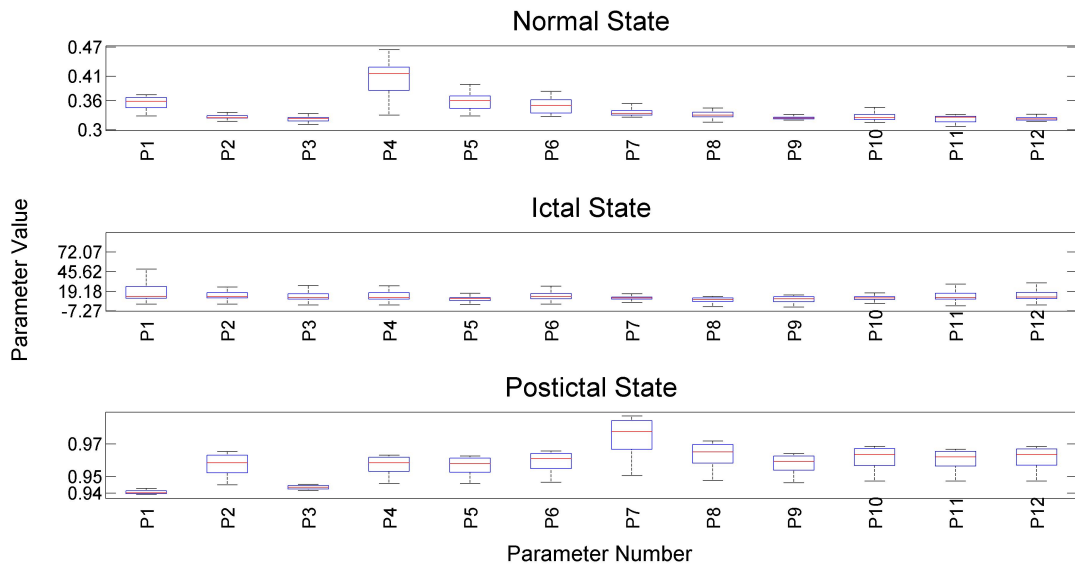
Figure 46: Subject 3, Treatment 1, Right Frontal: Values of Parameters during the three various EEG states

Figure 47: Subject 3, Treatment 1, Right Frontal : Normalized change in parameter indicates low activity correlation in the postictal state and high activity correlation in the ictal state between the areas; Power diagrams show high power in the ictal state and low power in the postictal state

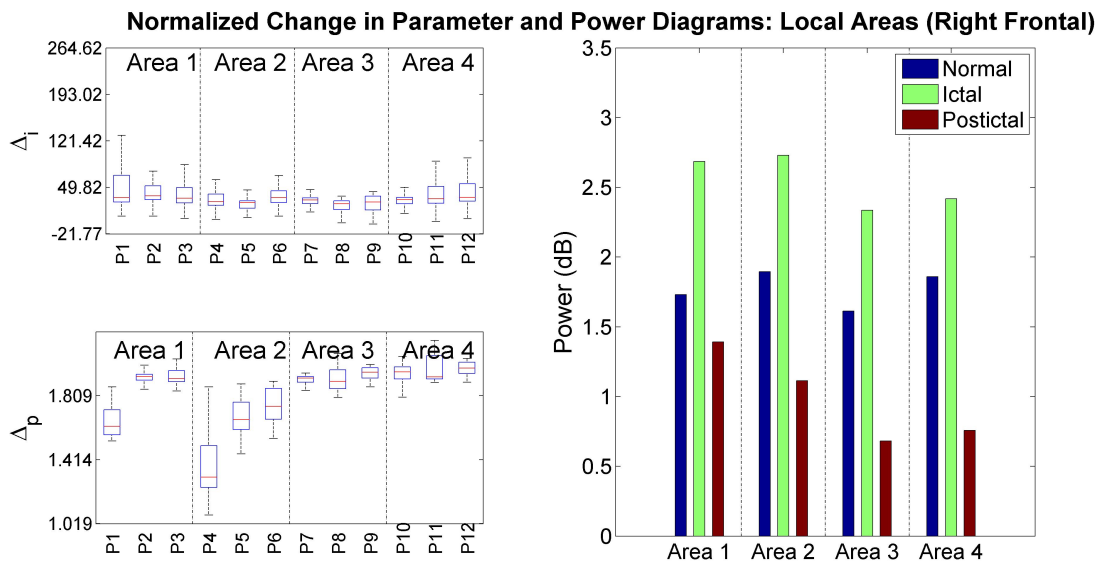Figure 48: Subject 3, Treatment 1, Left Frontal: Values of Parameters during the three various EEG states

Figure 49: Subject 3, Treatment 1, Left Frontal : Normalized change in parameter indicates low activity correlation in the postictal state and high activity correlation in the ictal state between the areas; Power diagrams show high power in the ictal state and low power in the postictal state

Figure 50: Subject 3, Treatment 1, Right Parietal: Values of Parameters during the three various EEG states

Figure 51: Subject 3, Treatment 1, Right Parietal : Normalized change in parameter indicates low activity correlation in the postictal state and high activity correlation in the ictal state between the areas; Power diagrams show high power in the ictal state and low power in the postictal state
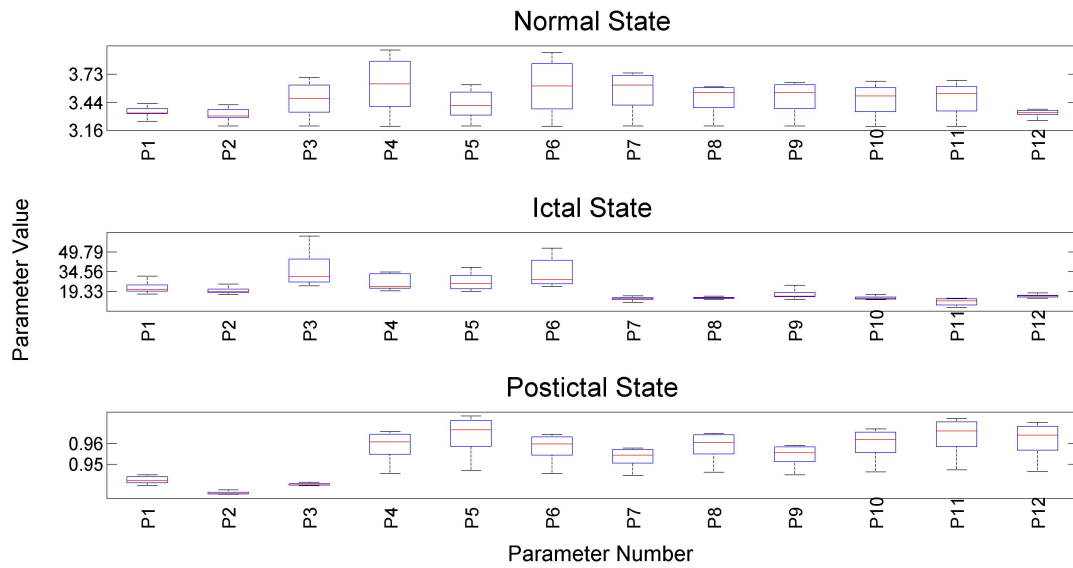
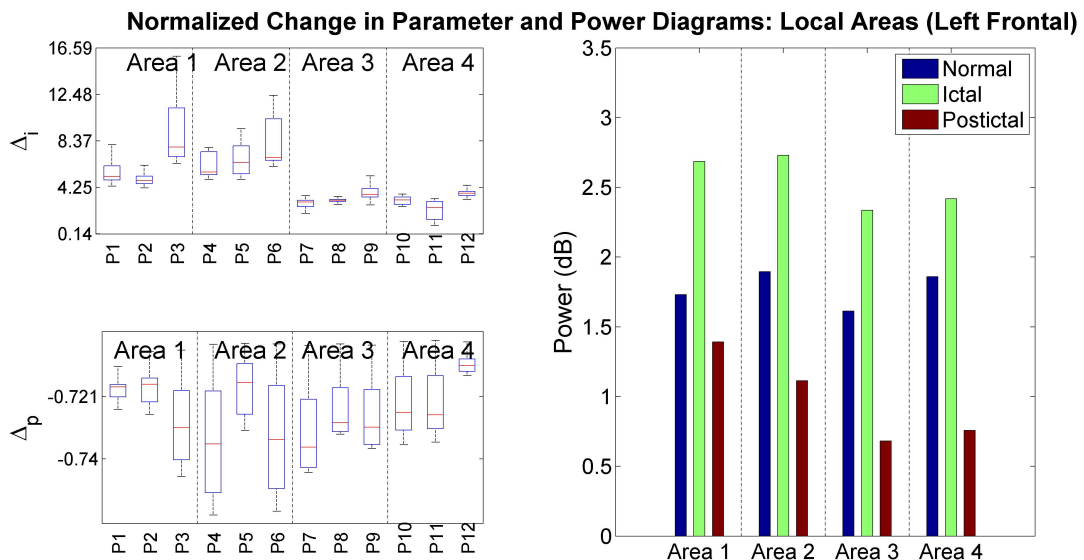Figure 52: Subject 3, Treatment 1, Left Parietal: Values of Parameters during the three various EEG states

Figure 53: Subject 3, Treatment 1, Left Parietal : Normalized change in parameter indicates low activity correlation in the postictal state and high activity correlation in the ictal state between the areas; Power diagrams show high power in the ictal state and low power in the postictal state
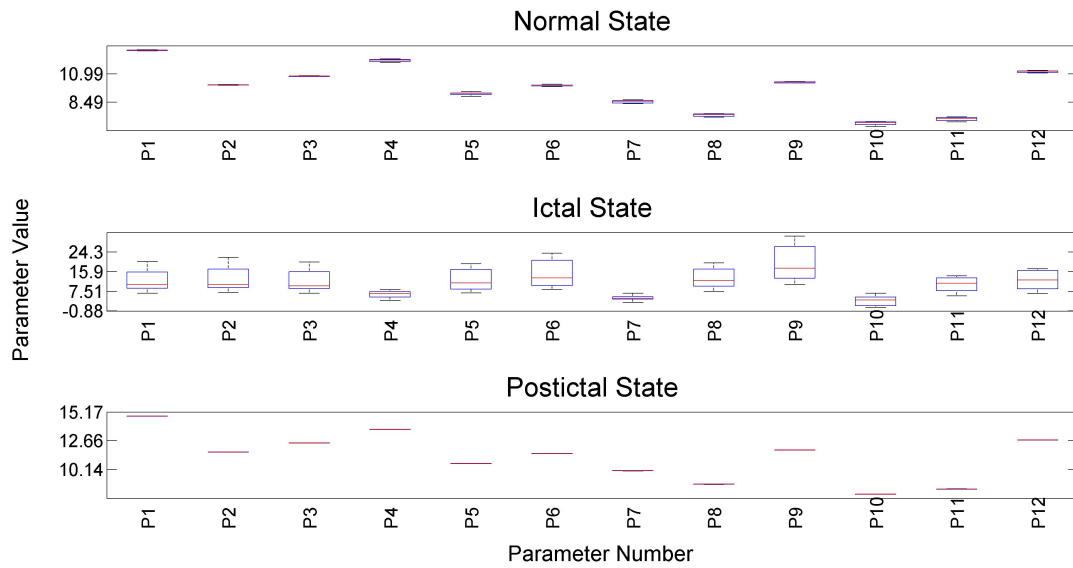
Figure 54: Subject 3, Treatment 2, Right Frontal: Values of Parameters during the three various EEG states

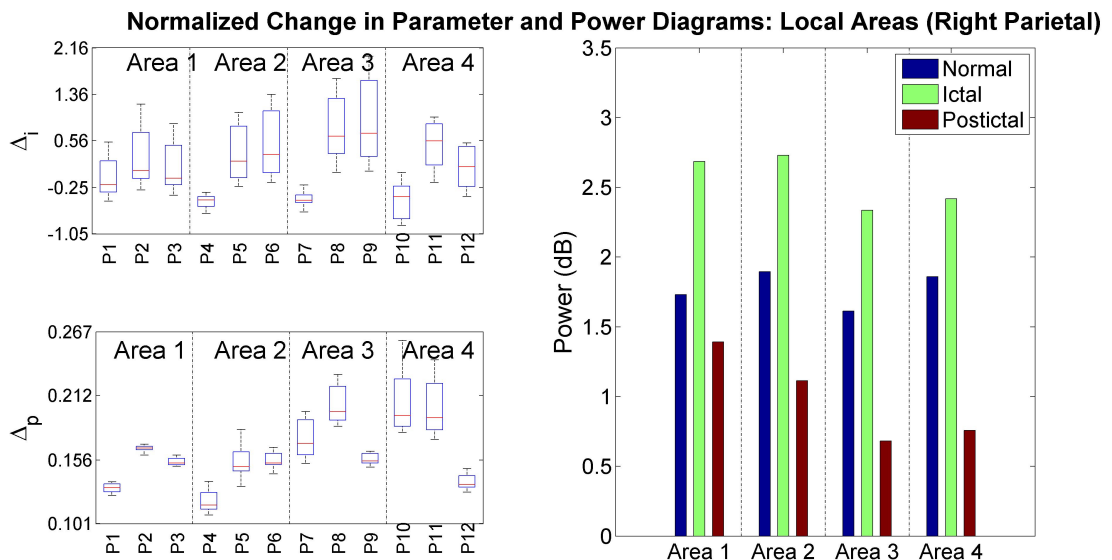Figure 55: Subject 3, Treatment 2, Right Frontal : Normalized change in parameter indicates low activity correlation in the postictal state and high activity correlation in the ictal state between the areas; Power diagrams show high power in the ictal state and low power in the postictal state
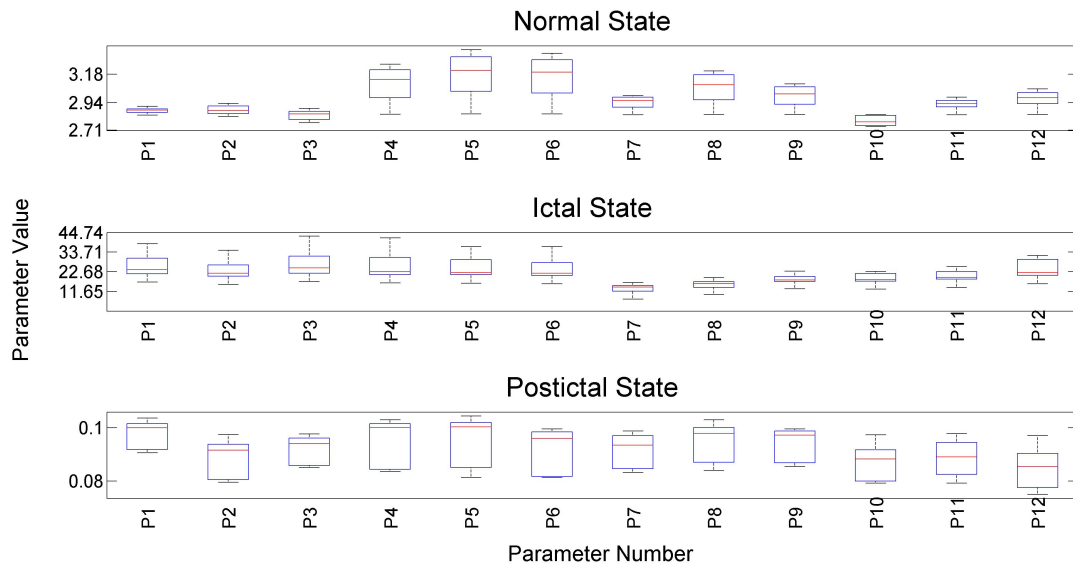
Figure 56: Subject 3, Treatment 2, Left Frontal: Values of Parameters during the three various EEG states
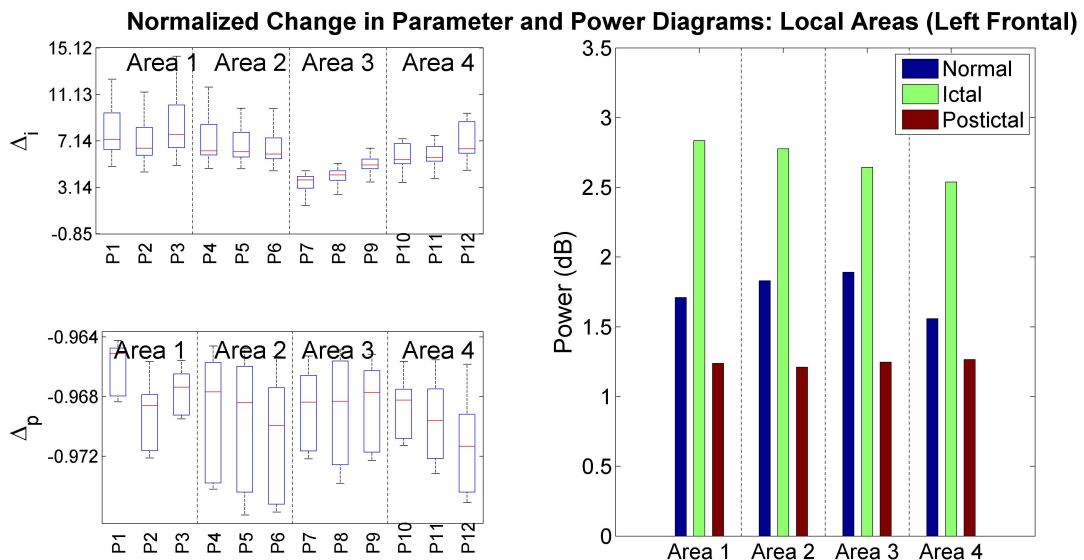
Figure 57: Subject 3, Treatment 2, Left Frontal : Normalized change in parameter indicates low activity correlation in the postictal state and high activity correlation in the ictal state between the areas; Power diagrams show high power in the ictal state and low power in the postictal state
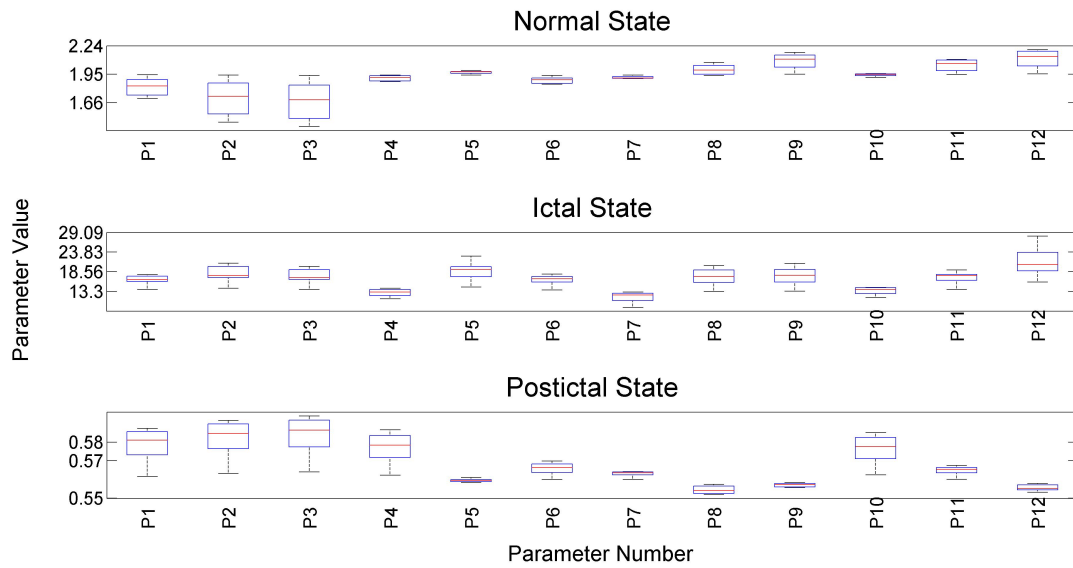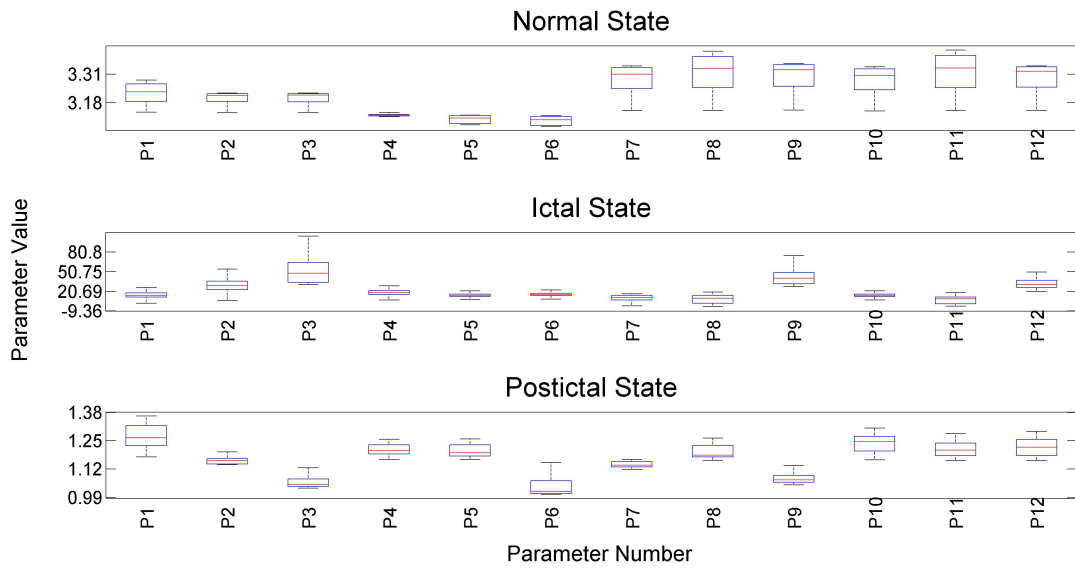
Figure 58: Subject 3, Treatment 2, Right Parietal: Values of Parameters during the three various EEG states
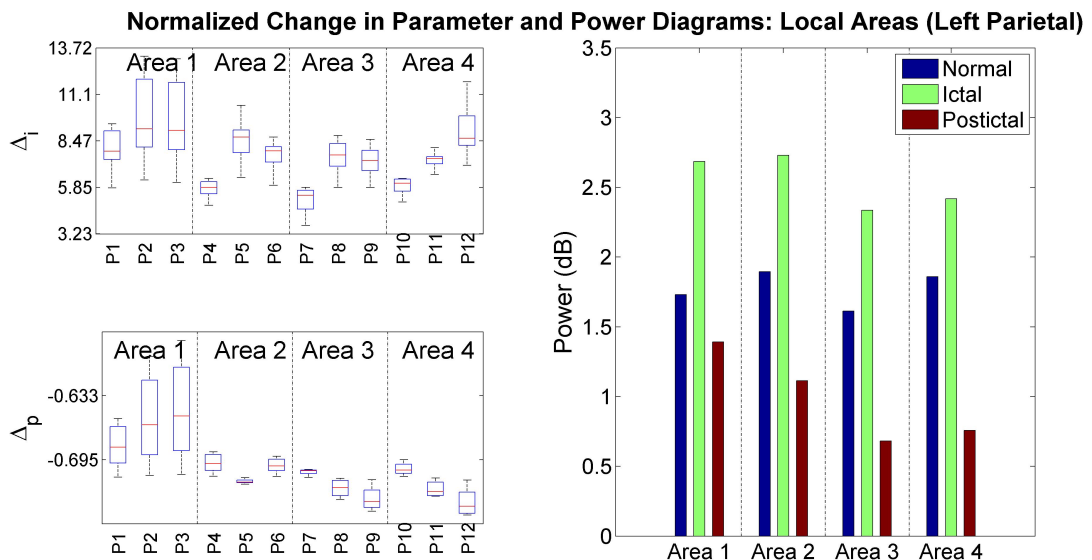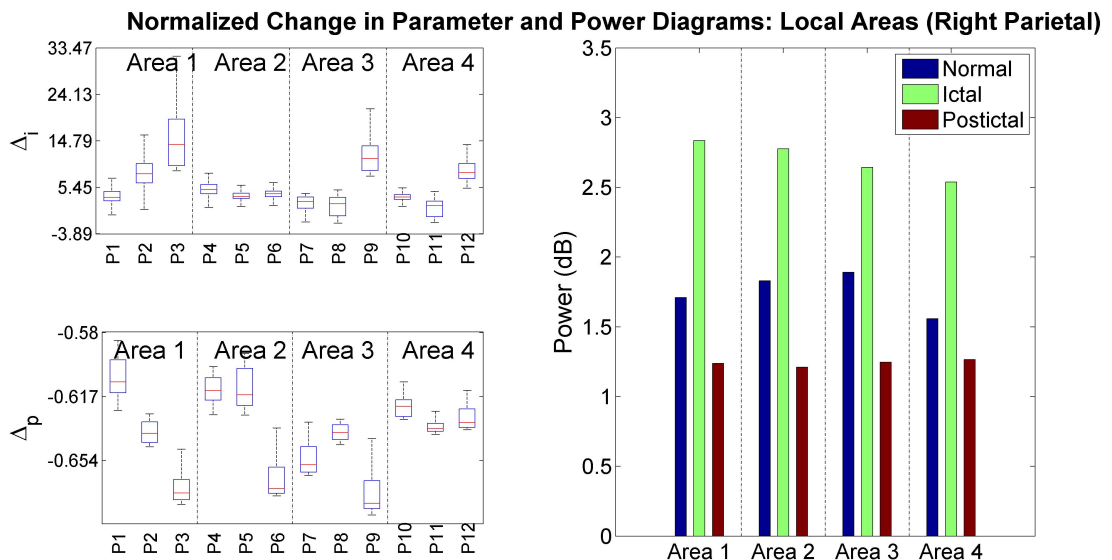

Figure 59: Subject 3, Treatment 2, Right Parietal : Normalized change in parameter indicates low activity correlation in the postictal state and high activity correlation in the ictal state between the areas; Power diagrams show high power in the ictal state and low power in the postictal state
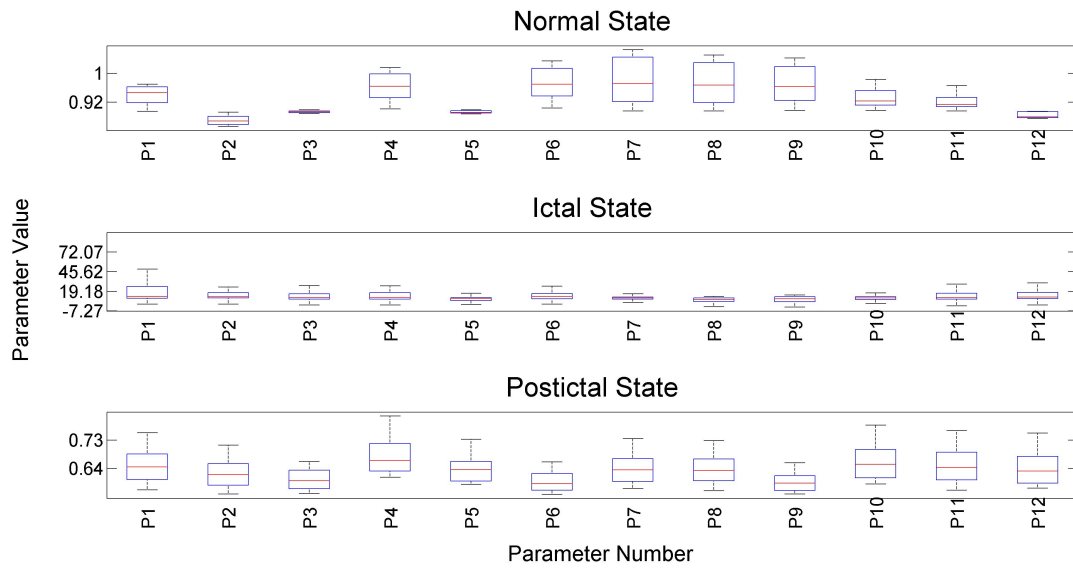
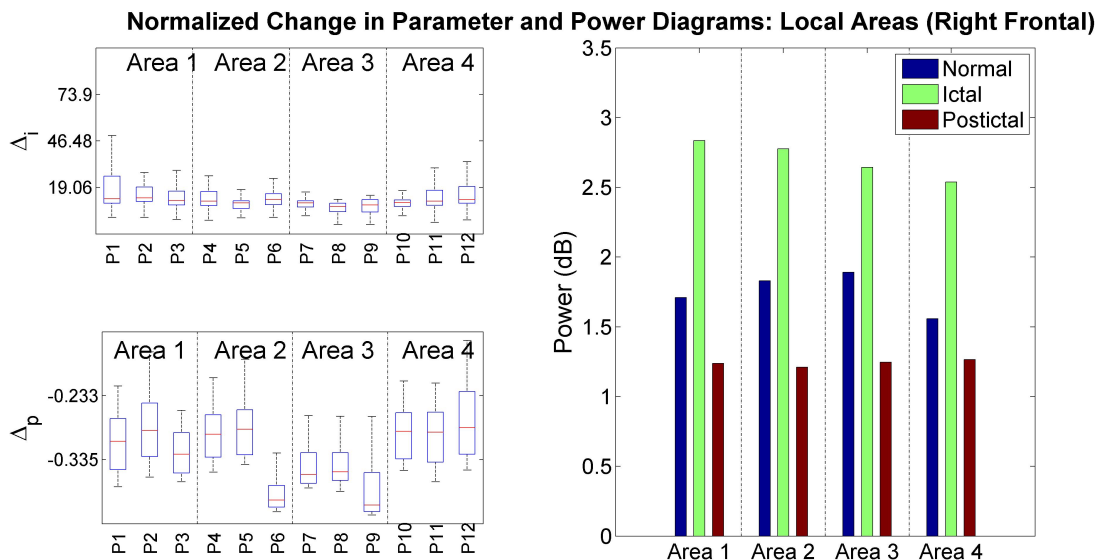Figure 60: Subject 3, Treatment 2, Left Parietal: Values of Parameters during the three various EEG states

Figure 61: Subject 3, Treatment 2, Left Parietal : Normalized change in parameter indicates low activity correlation in the postictal state and high activity correlation in the ictal state between the areas; Power diagrams show high power in the ictal state and low power in the postictal state
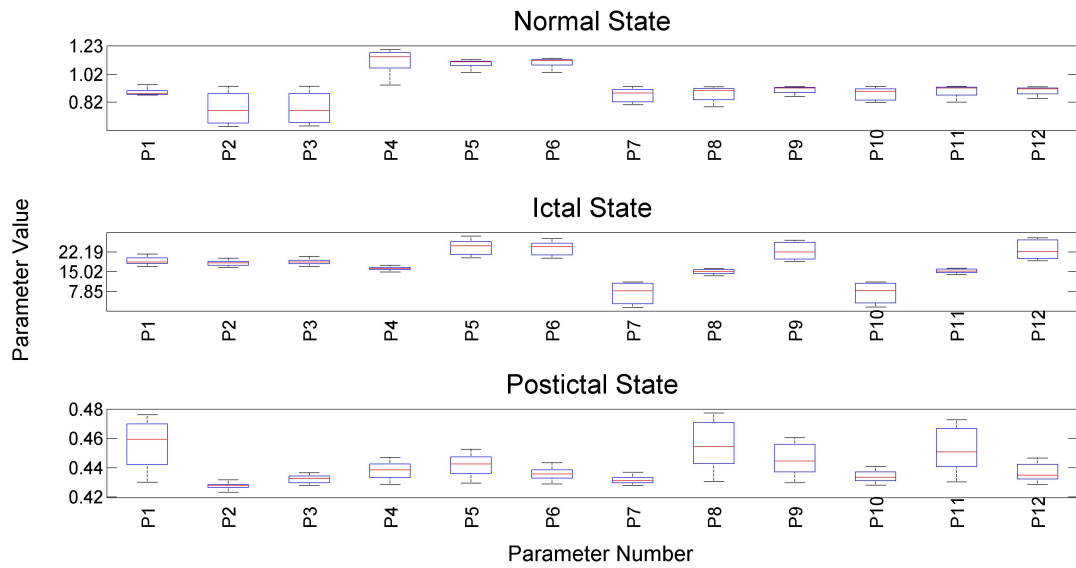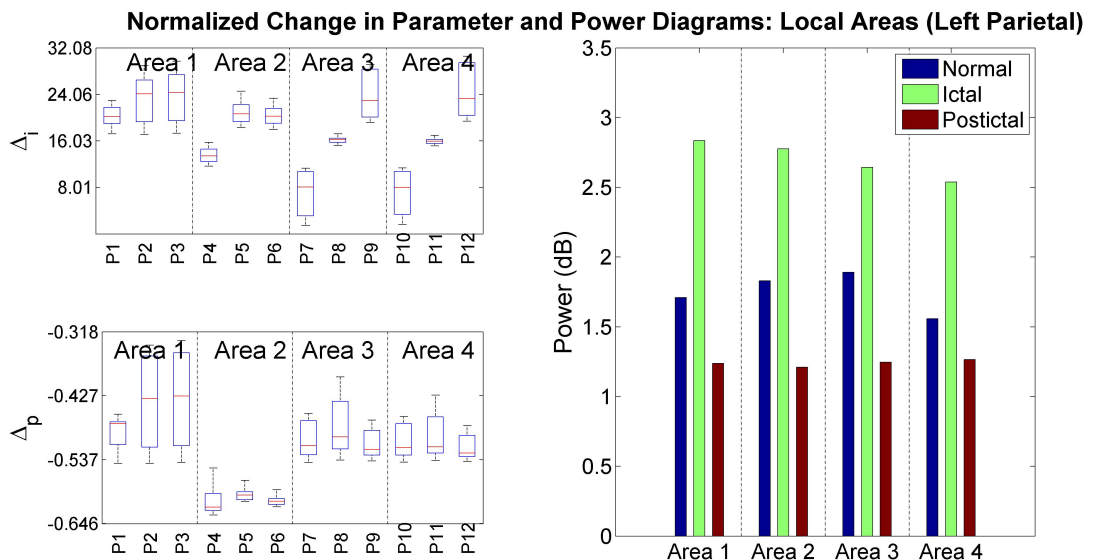
		Max	Min	Mean	Std Dev
Right Frontal	Treatment 1	251.6034	-8.75602	36.71733	28.64821
	Treatment 2	96.33266	-3.37224	12.83477	10.70419
Left Frontal	Treatment 1	2.018286	-0.90465	0.169958	0.615441
	Treatment 2	31.77601	-2.19211	5.782697	5.166159
Right Parietal	Treatment 1	15.84592	0.885662	5.061037	2.560878
	Treatment 2	14.3982	-0.12457	6.316076	2.179718
Left Parietal	Treatment 1	13.24522	3.703032	7.646297	1.826592
	Treatment 2	30.62539	1.4401	18.0189	6.588961

Table 20: Subject 3: Statistics of normalized change in parameter Δ_i during the ictal state for the local areas (Treatment 1 is reversed polarity)

		Max	Min	Mean	Std Dev
Right Frontal	Treatment 1	2.150941	1.07244	1.831479	0.199249
	Treatment 2	-0.14442	-0.42395	-0.31696	0.059085
		Max	Min	Mean	Std Dev
Left Frontal	Treatment 1	0.259693	0.108508	0.163509	0.030075
	Treatment 2	-0.58458	-0.6856	-0.63726	0.023704
		Max	Min	Mean	Std Dev
Right Parietal	Treatment 1	-0.70384	-0.75708	-0.72432	0.012559
	Treatment 2	-0.96424	-0.97594	-0.96912	0.003102
		Max	Min	Mean	Std Dev
Left Parietal	Treatment 1	-0.57977	-0.74815	-0.70181	0.032765
	Treatment 2	-0.33263	-0.6314	-0.51273	0.068736

Table 21: Subject 3: Statistics of normalized change in parameter Δ_p during the postictal state for the local areas (Treatment 1 is reversed polarity)

G. Conclusion

The parameters' values that we got are a measure of activity of neurons and of how these activities correlate to each other. In other words, they represent the functional connectivity which is a statement about the observed correlations: it does not provide any direct insight into how these correlations are mediated [14]. Specifically, the functional connectivity is defined as the temporal correlation between spatially remote neurophysiological events: it's a characterization of the functional interactions. Hence, our parameters refer to arbitrary relationships that might exist between the activation of the distinct separated neuronal populations and not the physical connections [15]. In this sense, our approach is similar to the so called generalized partial directed coherence (GPDC) as a measure for causal interaction between different brain areas [16]. The main distinction is that our work uses nonlinear biologically based models to infer functional connectivity.

As a general conclusion across subjects, we always have higher values of ictal parameters compared to normal parameters. This can be clearly seen in the different statistics tables where the mean of Δ_i is positive for all subjects. Thus, during a seizure the areas are highly correlated and produce a synchronized activity. On the other hand, during the postictal state the mean of Δ_p is almost always negative which indicates low parameters' values. Moreover, Δ_i in the local regions has higher values than the ones in the global regions.

In addition, as listed in Table 5 the configuration of electrodes in some sessions included a reverse polarity condition. For the same subject, the treatment with the reverse polarity showed higher Δ_p or less

connectivity/correlation between the 4 areas. .

Finally, looking at the power and the change in postictal parameters Δ_p in the local and global regions, we noticed that as the postictal power increases, Δ_p becomes more negative which means that there is less functional connectivity compared to the normal state. In that case we have more decoupling between the areas. On the other hand, when the postictal power decreases, there is is more functional connectivity. As mentioned earlier, the parameters do not model the physical connections between the areas but rather the correlation between their activities. Therefore, we can say that as the power decreases in the postictal state, each area activity is more correlated with the rest of the areas and can be predicted by the behavior of them. However, when we get a high power postictal state, the different activities are less correlated and cannot be predicted based on each other, which means that there are some other elements affecting their behavior.

As a future work, we definitely need more data to be able to generate more statistical confidence in the obtained parameter distibutions and get more general conclusions. In addition, we mainly focused on four global areas that are located far from each other thus the local areas need to be studied. These local, area-specific, functional models can provide a better insight to the efficacy of ECT protocols to modify the dominant activity within areas as it varies with the distance from stimulating ECT electrodes. At the modeling-estimation level, the nonlinear biologically inspired models for functional connectivity must be studied further as tools to address causal interactions between brain areas. The ECT modeling, here, is an excellent candidate to further explore this idea of how

77

various areas dynamically share common behavior across time and across experiments.

BIBLIOGRAPHY

[1] T. Spellman, A. V. Peterchev, and S. H. Lisanby. Erratum: Focal electrically administered seizure therapy: A novel form of ect illustrates the roles of current directionality, polarity, and electrode configuration in seizure induction (neuropsychopharmacology (2009) 34 (2002-2010) doi: 10.1038/npp.2009.12). *Neuropsychopharmacology*, 37(4):1077, 2012.

[2] Tammy D. Moscrip, Herbert S. Terrace, Harold A. Sackeim, and Sarah H. Lisanby. Randomized controlled trial of the cognitive side-effects of magnetic seizure therapy (mst) and electroconvulsive shock (ecs). *The International Journal of Neuropsychopharmacology*, 9(1):1–11, 2006.

[3] Mehul V Mankad, John L Beyer, Richard D Weiner, and Andrew Krystal. *Clinical manual of electroconvulsive therapy*. American Psychiatric Pub, 2010.

[4] Sandeep Grover, Surendra Kumar Mattoo, and Nitin Gupta. Theories on mechanism of action of electroconvulsive therapy. *German J Psychiatry*, 8:70–84, 2005.

[5] F Wendling, F Bartolomei, JJ Bellanger, and P Chauvel. Epileptic fast activity can be explained by a model of impaired gabaergic dendritic inhibition. *European Journal of Neuroscience*, 15(9):1499–1508, 2002.

[6] F N Karameh, M Awada, F Mourad, K Zahed, I Abou-Faycal, and Z Nahas. Modeling of neuronal population activation under electroconpulsive therapy.

[7] Hugh R Wilson and Jack D Cowan. Excitatory and inhibitory interactions in localized populations of model neurons. *Biophysical journal*, 12(1):1–24, 1972.

[8] BenH. Jansen and VincentG. Rit. Electroencephalogram and visual evoked potential generation in a mathematical model of coupled cortical columns. *Biological Cybernetics*, 73:357–366, 1995.

[9] F. S. Farzaneh, RA F. Rasoul Amir, S. S. Saeid, and K. A. Karim. A brief survey of computational models of normal and epileptic eeg signals: A guideline to model-based seizure prediction. *J Med Signals Sens*, 1(1):62–72, 01/01 2011.

[10] Simon Haykin. *Kalman Filtering and Neural Networks*. Wiley-Interscience, October 2001.

[11] Greg Welch and Gary Bishop. An introduction to the kalman filter, 1995.

[12] Ienkaran Arasaratnam and Simon Haykin. Cubature kalman filters. *Automatic Control, IEEE Transactions on*, 54(6):1254–1269, 2009.

[13] Ienkaran Arasaratnam and Simon Haykin. Cubature kalman smoothers. *Automatica*, 47(10):2245–2250, 2011.

[14] Karl J Friston. Functional and effective connectivity in neuroimaging: a synthesis. *Human brain mapping*, 2(1-2):56–78, 1994.

[15] Andreas A Ioannides. Dynamic functional connectivity. *Current Opinion in Neurobiology*, 17(2):161 – 170, 2007. Cognitive neuroscience.

[16] Martin Havlicek, Jiri Jan, Milan Brazdil, and Vince D Calhoun. Dynamic granger causality based on kalman filter for evaluation of functional network connectivity in fmri data. *Neuroimage*, 53(1):65–77, 2010.